Geophysical Journal International

Geophys. J. Int. (2010) **181,** 966–984 doi: 10.1111/j.1365-246X.2010.04551.x

Earthquake mechanisms and active tectonics of the Hellenic subduction zone

Beth Shaw and James Jackson

Bullard Laboratories, University of Cambridge, Cambridge, UK. E-mail: bs370@cam.ac.uk

Accepted 2010 February 4. Received 2009 December 7; in original form 2009 August 28

SUMMARY

We use improved focal mechanisms and centroid depth estimates of earthquakes, combined with GPS velocities, to examine the tectonics of the Hellenic subduction zone, and in particular the processes occurring at both ends of the Hellenic Arc. Nubia-Aegean convergence is accommodated by shallowly dipping thrust-faulting along the subduction–zone interface, as well as by steeper splay faults in the overriding material. From a comparison of observed and expected seismic moment release over the last 100 yr, combined with existing knowledge of the longer-term documented historical record, we confirm earlier suggestions that most (80 per cent) of this convergence is accommodated aseismically, that is, that the subduction zone is uncoupled. This conclusion is robust, even allowing for rare very large earthquakes on splay faults, such as that of AD 365, and also allowing for the contribution of small earthquakes. The downgoing Nubian plate deforms by arc-parallel contraction at all depths, from 200 km seaward of Crete to at least 100 km within the subducting slab. Extensional (T) axes of earthquakes are aligned downdip within the descending slab suggesting that, even if the aseismic prolongation of the slab has reached the 670 km mantle discontinuity, it does not transmit stresses to shallower depths. Shallow thrust-faulting earthquakes on the subduction interface show a divergence of slip vectors round the arc, and GPS measurements show that this is accommodated mainly by E–W extension on normal faults in the overriding Aegean material. The eastern end of the subduction zone, south of Rhodes, displays distributed deformation in the overriding material, including a mixture of strike-slip and splay-thrust faulting, and probably involves rotations about a vertical axes. Here slip on the interface itself is by thrust faulting with slip vectors oblique to the arc but parallel to the overall Nubia-Aegean convergence: there is no evidence for slip-partitioning in the traditional sense. In the west, the subduction zone terminates in a distributed zone of parallel NE–SW strike-slip faults, of which the most prominent is the Kefalonia Transform Fault (KTF). A flexural gravity anomaly confirms that the deep bathymetric escarpment of the KTF is a lateral ramp, formed as the Ionian islands are emplaced SW onto the Apulian lithosphere, and enhanced by minor thrust faulting with slip vectors perpendicular to the scarp. Distributed parallel strike-slip faults both SW and NE of mainland central Greece terminate in E–W graben in central Greece, which accommodate the overall NE–SW shear by clockwise block rotation. Central Greece therefore acts as a relay zone between the strike-slip faulting of the NE Aegean and the Ionian Islands–western Peloponnese.

Key words: Seismicity and tectonics; Subduction zone processes; Neotectonics.

1 INTRODUCTION

The Hellenic subduction zone is a key element in the active tectonics of the Eastern Mediterranean, yet many important details of its kinematics remain poorly understood. Mediterranean seafloor, of probable Mesozoic age (Chaumillon & Mascle 1995, 1997) subducts northwards beneath Crete at a rate (35 mm yr^{-1}) that greatly exceeds the convergence between Africa (Nubia) and Eurasia (5–10 mm yr^{-1}) because of the rapid SW motion of the southern Aegean itself, relative to Eurasia (McKenzie 1972; Reilinger *et al.* 2006). The surface morphology of the subduction system is obscured by a sedimentary section up to 10 km thick overlying the ocean crust, which is deformed in a broad accretionary prism south of Crete, known as the Mediterranean Ridge (Fig. 1; Le Pichon *et al.* 1979, 1982; Kenyon *et al.* 1982; Kastens *et al.* 1992; Foucher *et al.* 1993). A dramatic 2–3 km high,

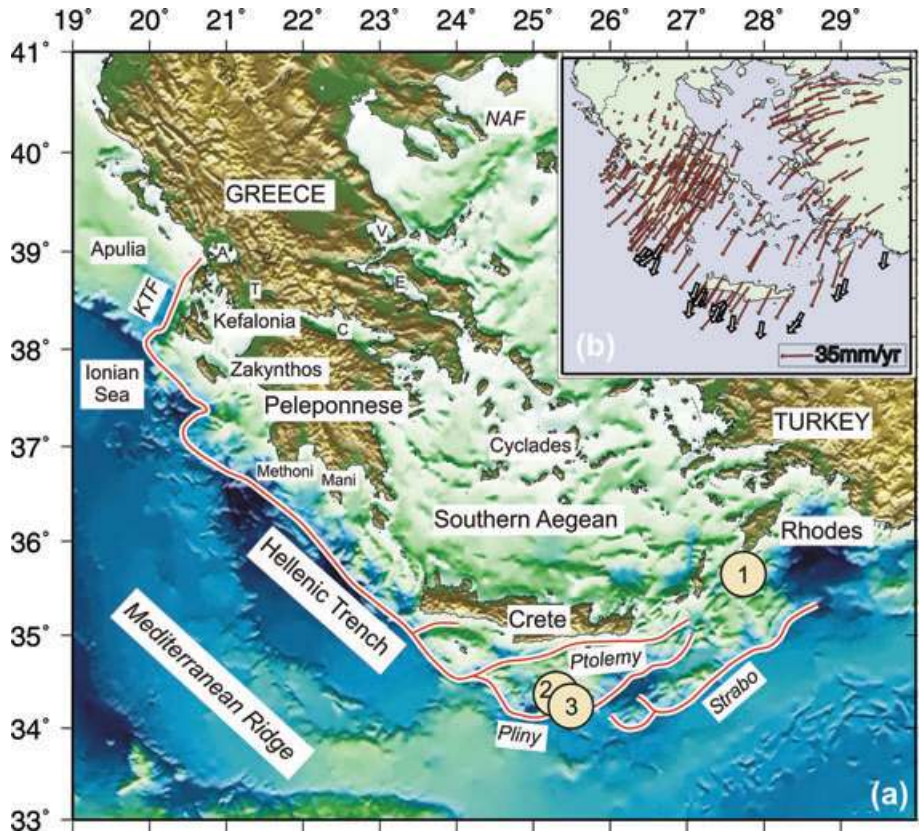

Figure 1. (a) The principal tectonic features and bathymetry-topography Smith & Sandwell (1997); Sandwell & Smith (2009) of the Hellenic Subduction Zone. The Hellenic Trench is a 4 km high escarpment, which branches into three deep trenches in the east, and terminates in the Kefalonia Transform Fault (KTF) in the west. The Mediterranean Ridge is a thick (up to 10 km) pile of sediment forming the accretionary prism of the subduction zone. The locations of the three example earthquakes are represented by yellow circles. The extensional graben of Central Greece are labelled as letters: C for Corinth; E for Evia; A for Arta; V for Volos; and T for Trichonis Lake. (b) Red arrows are GPS velocity vectors in the region relative to Nubia (see text). Slip vectors of thrust-faulting earthquakes along the subduction interface and on splay thrust faults in the overriding material are plotted as white arrows.

south-facing bathymetric scarp runs in an arc between the Peloponnese and Crete, splitting into at least three branches south of Crete, and continuing east to Rhodes as the Ptolemy, Pliny and Strabo trenches (Fig. 1; McKenzie 1978; Le Pichon *et al.* 1979; Kreemer & Chamot-Rooke 2004). Although this scarp is referred to by us, and others, as the Hellenic Trench, it is clearly not the expression of an oceanic trench in the usual sense, as the earthquakes directly beneath it are low-angle thrusts at depths of 20–40 km (Taymaz *et al.* 1990), and it is not the site where those thrusts would project to the surface. Assuming those thrusts represent the interface between the downgoing African lithosphere and the overriding Aegean, that interface would instead project to the surface at least 150 km south of Crete, beneath the aseismic Mediterranean Ridge. In fact, it is more likely that the interface never reaches the surface at the Mediterranean Ridge at all, but is 'blind', and dissipates the motion in sediment thickening and folding instead. The escarpment of the Hellenic Trench may thus be a backstop to the deformed accretionary prism, where seafloor sediments that are decoupled aseismically from the oceanic crust by weak layers, including Messinian salt and lower Cretaceous shales (Camerlenghi *et al.* 1992; Mascle & Chaumillon 1998), abut against the continental crust of Crete and the Aegean (e.g. Angelier *et al.* 1982; Le Pichon 1982). It is probable that the scarp of the Hellenic Trench is the surface expression of a steep (∼30°) reverse fault splaying off the deeper underlying thrust-fault interface of the subduction zone (Shaw *et al.* 2008); an inference we discuss more later.

Where surface features are obscured or complicated, the obvious recourse is to look at earthquake focal mechanisms. The Global CMT catalogue, and other compilations (e.g. Papazachos *et al.* 2000; Kiratzi & Louvari 2003; Benetatos *et al.* 2004), show a bewildering variety of mechanisms associated with the subduction; indicating normal, thrust and strike-slip fault-plane solutions with a range of orientations all apparently in nearly the same place. Taymaz *et al.* (1990) showed that the way to clarify this information was through careful quality control of the earthquake data. Using body-waveform modelling to improve and constrain focal mechanisms and, especially, centroid depths, they exposed a clear pattern, revealing that the earthquakes near Crete split into three groups. The Nubia-Aegean convergence itself is achieved by low-angle (10–20°) thrust faults with steeper reverse-fault splays at shallower depths above them. The overriding Aegean crust has mechanisms that involve arc-parallel extension, mostly by normal faulting. The underthrusting African lithosphere undergoes arc-parallel shortening, achieved by both thrust and strike-slip faulting.

The crustal structure and lithospheric structure in the area of Crete has been studied using wide aperture seismic data (Bohnhoff *et al.* 2001), receiver functions and Rayleigh phase velocities (Endrun *et al.* 2004). These studies reveal a slab that dips to the North beneath Crete. Endrun *et al.* (2004) show that the average depth of the subducted oceanic Moho is 55 km beneath the island of Crete.

A lack of earthquakes elsewhere restricted the Taymaz *et al.* (1990) study to the area around Crete. Since then, the greatly

increased earthquake data set, combined with excellent GPS data (see Section 3.3), potentially allow us to see whether the pattern found by Taymaz *et al.* (1990) near Crete is representative of the whole arc, and to interpret the earthquake focal mechanisms, depths, slip vectors and *P*- and *T*-axes in their geodynamic context. These are the broad aims of this paper. One interest concerns the extent to which the pattern itself, in general, is related to the strong curvature of the arc. Particular questions are associated with the western and eastern ends. In the west, the subduction zone terminates where the downgoing side changes along strike from the oceanic crust of the Ionian Sea to the continental crust of the Adriatic and Apulia (Fig. 1). This change involves a right-step from the Ionian islands to the NW coast of Greece, and is associated with a major strike-slip fault, sometimes called the Kefalonia Transform Fault (KTF, e.g. Louvari *et al.* 1999), though it is also associated with thrust faulting, coastal uplift and a general decrease of earthquake depths. This western termination is one of the most seismically active parts of Greece, yet its kinematics are not well understood. The eastern termination of the subduction zone is also obscure. GPS observations show that, near Rhodes, the convergence direction is highly oblique to the Ptolemy, Pliny and Strabo trenches, suggesting that the zone must involve a substantial strike-slip component to the convergence (Fig. 1), but a lack of earthquakes has left this region almost untouched by earlier studies, beyond speculation about possible partitioning of the convergence onto parallel strike-slip and thrust faults, as is indeed common elsewhere in the oceans. (In the context of this paper, we take 'partitioning' to mean that oblique convergence is separated into perpendicular strike-slip and thrusting components, which are taken up on parallel faults.) These kinematic questions are primary foci of this paper.

An additional oddity of the Hellenic subduction zone is that it is known to be largely aseismic, in the sense that there are not enough earthquakes to account for the Africa-Aegean convergence (Jackson & McKenzie 1988). This is hinted at by an assessment of the last 100 yr quantitative instrumental data, which accounts for a maximum of 15 per cent of the known convergence, but becomes even more likely when combined with the known historical record. The 100 yr seismic deficit requires an earthquake of M_w 8 every 14 yr, or one of M_w 7.1 every year, to rectify the situation; there is simply no suggestion of this extreme level of activity in the historically documented record (Ambraseys *et al.* 1995; Guidoboni & Comastri 2005; Ambraseys 2009). Yet the historical record *does* contain two earthquakes of $M_w > 8$ in the last 2000 yr, each of which must have had a source dimension of greater than 100 km (Ambraseys 1962; Papazachos 1996; Guidoboni & Comastri 1997; Stiros & Drakos 2006; Shaw *et al.* 2008). These two earthquakes are not nearly large enough or frequent enough to account for the missing seismic moment: together they can only account for an extra 5–10 per cent of the expected moment over 2000 yr. However they raise a paradox: it is easy to understand how a largely aseismically slipping interface may produce occasional earthquakes of M_w 6, with source dimensions of about 10 km, on a few locked patches; but it is harder to see how the same interface can be both 75 per cent aseismic and also be capable of accumulating strain over a sufficiently large area to generate earthquakes of $M_s > 8$ (Kanamori 1977; Ruff & Kanamori 1983).

Shaw *et al.* (2008) suggested a resolution of this paradox, in which rare M_w 8 earthquakes are generated on high-angle splays off the main subduction interface at depth. These splay faults account for 5–10 per cent of the convergence, while the bulk (90 per cent) of the convergence is accommodated updip on the main interface itself, nearly all of it by aseismic slip with small local patches slipping in earthquakes of up to about M_w 6.0. In this description only the 5–10 per cent of the convergence accommodated by the high-angle splays is fully coupled and stores significant elastic strain; the remainder is largely uncoupled. This conclusion is supported by GPS measurements that show only 1 mm yr^{-1} of shortening between Crete and the Cyclades. (These arguments are quantified further in the Appendix, where we show that that Ganas & Parson's (2009) claim that the Hellenic subduction zone is fully coupled cannot be correct.) As evidence for their interpretation of the faulting, Shaw *et al.* (2008) used their forensic study of the uplift of Crete in the M_w 8.4 AD 365 earthquake, suggesting also that such splays account for the presence of the Hellenic Trench bathymetric escarpment itself, as well as the uplift and tilting of Crete. By contrast, slip along the subduction zone interface itself can only produce the observed AD 365 uplift if slip extends to implausibly great depths (around 70 km), and if the fault slips by improbably large amounts (40–50 m), as shown by Stiros & Drakos (2006), Ganas & Parsons (2009) and Shaw *et al.* (2008). If correct, Shaw *et al.*'s interpretation of the AD 365 event and the faulting near Crete has important implications for the earthquake and tsunami hazard of the eastern Mediterranean, and other large-earthquake-prone regions of the subduction zone could be identified by examination of the earthquake focal mechanisms and depths, and of the geomorphology of any adjacent land. This is an additional motivation for the present study.

The bulk of this paper is concerned with detailed examination of earthquake focal mechanisms, depths and slip vectors and their comparison with GPS observations. These are considered round the arc in groups (1) within the subducting lithosphere, (2) on the interface and (3) within the overriding Aegean. Special consideration is given to the western and eastern subduction zone terminations, followed by a summary of the implications of the study for the overall tectonics of the region.

2 DATA AND METHODS

2.1 Earthquake epicentres

To make correct associations of earthquakes with tectonic features it is important to use epicentres that are as accurate as possible. Except for the most recent events, for which only USGS PDE epicentres are available, we use epicentres determined in Engdahl *et al.* (1998) and their updated catalogues (ISC locations are used for events before 1964). With the obviously complicated velocity structure of a subduction zone, and the uneven station distribution contrasting dense coverage in Europe and Asia to the north with sparse coverage in Africa and the oceans to the south, epicentre bias and inaccuracy are potential issues (Ambraseys 1978; Berberian 1979).

To assess the scale of epicentral mislocation, we found six earthquakes that were located both by the global teleseismic network and by dense temporary local seismograph networks in central Greece, the Peloponnese and Crete (Hatzfeld *et al.* 1990, 1993; Meier *et al.* 2004). A comparison between the two locations for each earthquake shows a difference of less than 12 km in all cases, with no consistent pattern in the azimuths of offset (Table 1). A distance of 10–15 km is roughly equivalent to the rupture length of a M_w 6.0 earthquake. The size of symbols used to represent earthquakes in maps in this paper is large compared with this uncertainty in epicentral location, so the true location is likely to lie within the symbol. Our subsequent interpretations are not sensitive to errors of this scale.

Table 1. Comparison between (Engdahl *et al.* 1998) locations, and locations using dense local seismic networks.

Date	Time	Lat	Long	M_w	Δd (km)	Offset azimuth ° from N	Source
971105	12:22:56	34.8	24.0	4.5	1	117°	Meier *et al.* (2004)
880712	02:26:53	38.7	23.4	4.4	6	123°	Hatzfeld *et al.* (1993)
880727	05:00:13	35.4	24.8	4.1	11	186°	Hatzfeld *et al.* (1993)
860608	04:54:52	36.0	21.5	5.3	10	131°	Hatzfeld *et al.* (1990)
860614	17:50:22	36.0	22.0	4.7	11	91°	Hatzfeld *et al.* (1990)
860619	15:14:45	36.6	21.2	4.7	11	30°	Hatzfeld *et al.* (1990)
860705	09:52:45	37.9	22.5	4.2	7	277°	Hatzfeld *et al.* (1990)

2.2 Focal mechanisms, slip vectors and depths

The primary interest of this paper is in the focal mechanisms and depths of earthquakes larger than $M_w \sim 5.2$. The best constraints on these parameters come from long-period teleseismic body wave modelling, which can provide considerable improvements over routine global CMT catalogue (CMT 2009) determinations, especially for centroid depths (Maggi *et al.* 2000b; Talebian & Jackson 2004; Engdahl *et al.* 2006).

In our modelling procedure we used *P* and *SH* body waves recorded by stations of the Global Digital Seismic Network (GDSN). Seismograms in the teleseismic distance range of 30–90° were first convolved with a filter that reproduces the bandwidth of the old WWSSN 15–100 long-period instruments. At these periods the source of earthquakes of $\sim M_w$ 6 appears as a point in space (the centroid) with a finite rupture time, and the seismograms are sensitive to the source parameters of the centroid while relatively insensitive to the details of geological structure. We then used the MT5 version (Zwick *et al.* 1994) of McCaffrey & Abers (1988)'s and McCaffrey *et al.* (1991)'s algorithm, which inverts the *P* and *SH* waveform data to obtain the strike, dip, rake, centroid depth, seismic moment and the source time function, which is parametrized by a series of isosceles triangle elements of half-duration τ s. Wherever possible we used the observed onset time on the high-frequency broad-band records to align the observed and synthetic waveforms. We always constrained the source to be a double-couple. Stations are weighted by azimuth density, and then the weights of *SH* waveforms are halved to compensate for their generally larger amplitudes. The method and approach we used are described in detail elsewhere (e.g. Nabelek 1984; McCaffrey & Nabelek 1987; Molnar & Lyon-Caen 1989; Taymaz *et al.* 1991) and are too routine to justify detailed repetition here.

A simple source-region velocity structure was specified, using up to a maximum of two layers and a water layer. This permits a different average velocity above the source (which determines the delay between direct and surface-reflected arrivals, and hence depth) from that below the source (which controls station positions on the focal sphere). The source itself is always in the underlying half-space. To comply with these requirements, the source structures we chose followed the approach of Taymaz *et al.* (1990) to ensure direct comparison with their results. For the events that are relatively shallow, typically around 20 km, and south of the Hellenic Trench escarpment, we used a structure consisting of a layer 8 km thick with V_p 4.5 km s^{-1}, representing the sediment covering the seafloor, overlying a half-space of V_p 6.5 km s^{-1}. For those with a centroid depth around 40 km or greater, we used a 24 km thick layer of V_p 6.5 km s^{-1} overlying a half-space of V_p 7.8 km s^{-1}. For all offshore earthquakes we included a water layer of depth appropriate to their Engdahl *et al.* (1998) locations. As Taymaz *et al.* (1990) showed, small variations in the velocity structure used do not significantly affect the focal mechanism and are responsible for depth uncertainties of up to ±4 km. We are therefore confident in assimilating mechanisms and depths from other similar waveform-based studies where slightly different velocity structures have been used (e.g. Benetatos *et al.* 2004).

The earthquake mechanisms and depths we discuss in this paper are ranked in quality by category. The best (in red) are those whose source parameters are independently determined by long-period body wave modelling and with good *P* and *SH* waveform coverage. The formal errors associated with the minimum-misfit solution obtained by the inversion algorithm underestimate the true uncertainties in the source parameters (e.g. Molnar & Lyon-Caen 1989). A better estimate of uncertainties is found by fixing some of the source parameters at values close to but different from those of the minimum misfit solution, and seeing whether the match of the observed to synthetic seismograms deteriorates (Molnar & Lyon-Caen 1989; Taymaz *et al.* 1991; Maggi *et al.* 2000b). Such sensitivity analyses showed that for the best-determined earthquakes (in red) the uncertainties are typically ±15° in strike, ±5° in dip, ±20° in rake and ±4 km in depth. Earthquakes with less waveform data, or with inferior station coverage, but whose centroid depths are nonetheless well constrained by body wave modelling are shown in pink, often adopting the best-double-couple CMT focal mechanism. In grey we include best-double-couple CMT mechanisms of earthquakes for which there is insufficient data, or for which the data is of too poor quality, to carry out independent waveform modelling at all; for these earthquakes we have no accurate depth control. Finally, some of the most reliable first-motion fault-plane solutions, determined from long-period records of the WWSSN in earlier studies by McKenzie (1972, 1978) are also plotted to extend our coverage back in time to the early 1960s; but for these earthquakes also there is no accurate depth control. The focal mechanism data and, where available, the improved centroid depth estimates, for all earthquakes are listed in tables in the Supporting Information.

We illustrate below (Section 3.4) the importance of this careful forensic approach to evaluating focal mechanisms and depths with three examples. In each case the accurate mechanisms and depths reveal or confirm the tectonic significance of the earthquakes, which could otherwise easily be misinterpreted, or would not be known with confidence.

2.3 GPS data

The GPS velocities used here are taken from the data sets of Reilinger *et al.* (2006) (Greece only) and Hollenstein *et al.* (2008), which have been combined with the velocities obtained by the COMET group (M. Floyd, personal communication). For most of the purposes of this paper, these velocities have been rotated into a Nubian frame of reference (after Altamimi *et al.* 2007).

2.4 Example 1: Eastern Hellenic Arc, 2008 July 15

On 2008 July 15, a strike-slip earthquake of M_w 6.2 occurred in the eastern part of the subduction zone, south of Rhodes (see Fig. 1). In this region, the trend of bathymetric scarps offshore is oblique rather than perpendicular to the direction of convergence between the Aegean and Africa (Fig. 1), suggesting two possible fault configurations that could achieve the overall motion: either partitioning of the oblique left-lateral convergence onto separate pure thrust and strike-slip faults, or oblique slip on the main subduction zone interface.

The synthetic and observed waveforms for this event are shown in Fig. 2. The nodal planes are well determined by the available *P* and SH station distribution, and the depth is well constrained by the clear surface reflections in both *P* and *SH* waves. The left-lateral nodal plane strikes E–W, rather than NE–SW and parallel to the strike of the subduction zone at this point, as would be expected for a partitioned strike-slip component of oblique convergence. In addition, the depth of 56 ± 4 km suggests the event is in the downgoing African lithosphere, as we show later that the subduction interface itself is only seismogenic to about 40–45 km depth.

The *P* axis for this earthquake does trend NE–SW, and in fact this event is one of several within the downgoing African lithosphere that has a *P* axis parallel to the strike of the subduction zone. This is a pattern noted near Crete by Taymaz *et al.* (1990) that, we show later, continues round the whole arc, and may be related to the strong curvature imposed on the downgoing African Plate. The reason we have confidence in attributing this earthquake to that group is because we have confidence in the focal mechanism and depth.

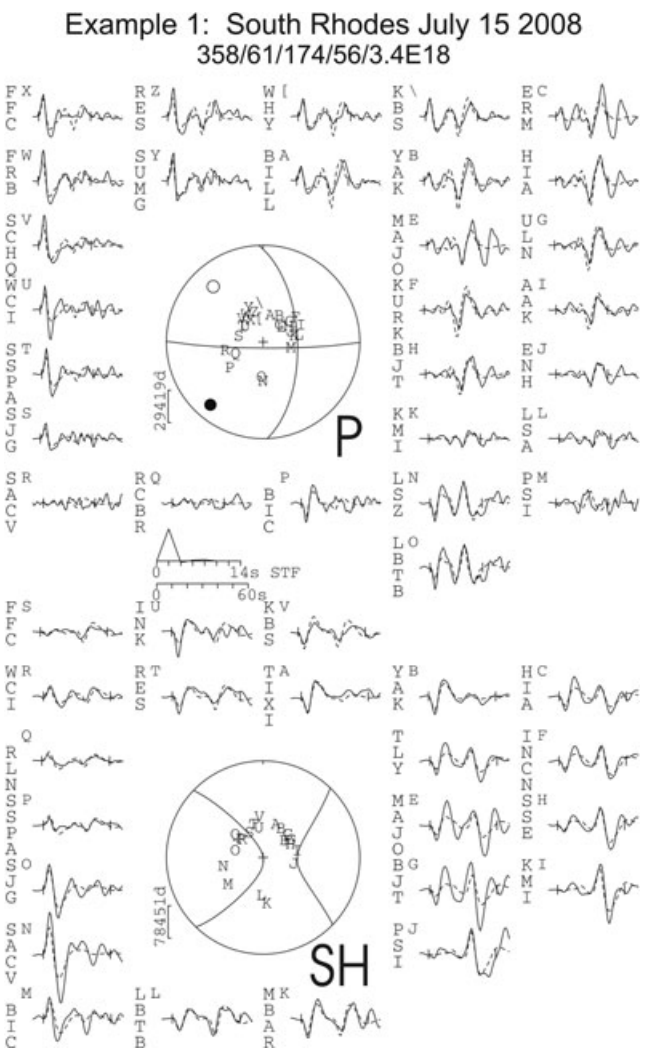

Figure 2. *P* and *SH* waveforms for earthquake example 1, south of Rhodes on 2008 July 15. Although it has a strike-slip mechanism, it is not related to the oblique convergence between Nubia and the Aegean, but rather represents along-arc shortening in the downgoing Nubian plate. The event header shows the strike, dip, rake, centroid depth and scalar seismic moment (in N m) of the minimum misfit solution. The top focal sphere shows the lower hemisphere stereographic projection of the *P* waveform nodal planes, and the positions of the seismic stations used in the modelling routine. The lower focal sphere shows the *SH* nodal planes. Capital letters next to the station codes correspond to the position on the focal sphere. These are ordered clockwise by azimuth, starting at north. The solid lines are the observed waveforms, and the dashed lines are the synthetics. The inversion window is marked by vertical lines on each waveform. The source time function (STF) is shown, along with the time scale for the waveforms. The amplitude scales for the waveforms are shown below each focal sphere. The *P*- and *T*-axes within the *P* waveform focal sphere are shown by a solid and an open circle, respectively.

2.5 Examples 2 and 3: shallow and steep thrust faulting earthquakes

An important feature of the Hellenic subduction zone is that the clear bathymetric feature known as the Hellenic Trench is not the surface expression of the main subduction interface. The true geometry and location of that interface is obscured beneath thick piles of sediment which deform and slide down bathymetric gradients. We show in section 5 that the larger earthquakes on the subduction interface are at depths of 15–45 km beneath the Hellenic Trench system, similar to the 20–40 km deep interface inferred to exist from microearthquakes (Meier *et al.* 2004) and larger earthquakes (Taymaz *et al.* 1990) beneath western and central Crete. Seismograms from one such earthquake (Example 2), which occurred on 2008 March 28 to the south of Crete (Fig. 1), are plotted in Fig. 3 (first two rows). The figure offers a visual comparison of the quality of the fit to the waveforms for synthetics generated at the best fitting depth (43 km) and at a much shallower depth (9 km) for the best-fitting fault-plane solution. The fit to the waveforms is severely degraded if the centroid depth is forced to be shallow. In this area, Bohnhoff *et al.* (2001) use wide-angle seismic data to infer an interface at 20–25 km, which they interpret to be the subduction zone interface in this region. However we suspect that this earthquake at 43 ± 4 km depth occurred on the subduction zone interface because: (1) it has a shallowly dipping thrust mechanism; (2) it has a slip vector that is parallel to the GPS-measured motion between the Aegean and Nubia in this region and (3) it occurs at almost exactly the same depth as other interface events to the SW of Crete (which are in a similar position relative to the main bathymetric escarpment of the Hellenic trench system). The alternative is that this earthquake occurred in the downgoing Nubian lithosphere but, as we show later, nearly all other earthquakes in the downgoing lithosphere have *P*-axes that are arc-parallel (showing contraction along the arc), whereas this earthquake has a *P*-axis that is perpendicular to the arc.

Another thrust-faulting earthquake occurred in the same part of Hellenic subduction zone on 2009 July 7, about 20 km east of the interface earthquake described above (Example 3, Fig. 1). This earthquake, of M_w 6.4, has a shallow centroid depth (9 km) and a plane which dips to the north at 30° (slightly steeper than the 20–25° dip of the subduction zone interface in this area). Seismograms at

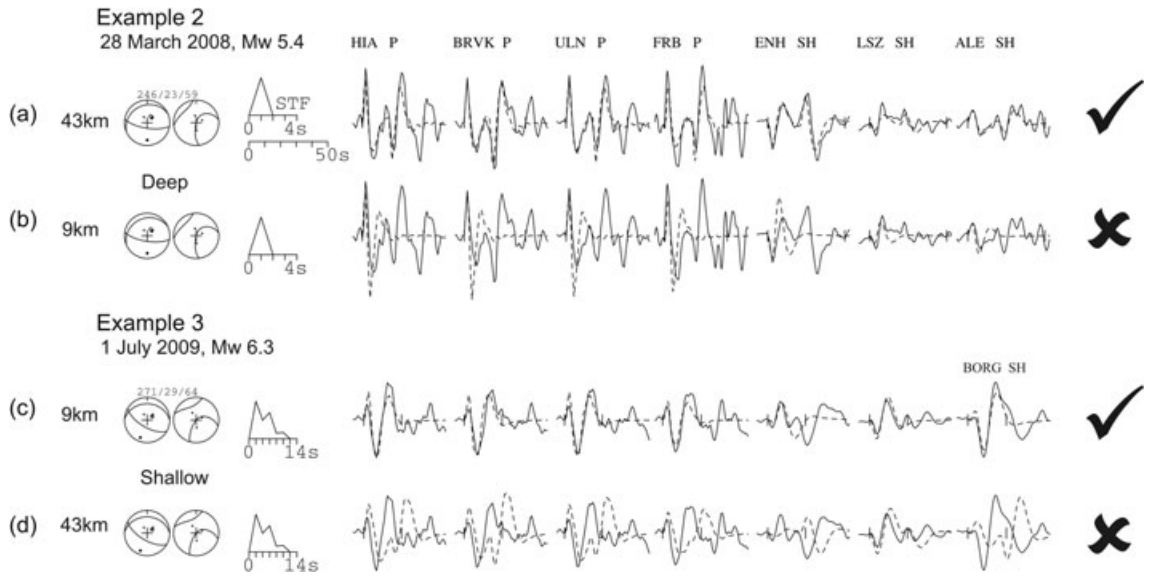

Figure 3. *P* and *SH* waveforms recorded at seven stations (4P, 3SH) for two earthquakes that occurred within about 20 km of each other on 2008 March 28 (example 2) and 2009 July 1 (example 3). Both involved thrust faulting, but one occurred at 43 km depth, along the subduction zone interface, whilst the other occurred at a depth of 9 km. Synthetics are calculated for both events at a depth of 9 km (b and c) and 43 km (a and d). The fit of observed (solid) to synthetic (dashed) waveforms is good in (a) and (c) and poor in (b) and (d), confirming their different depths.

selected stations are matched much better by synthetics calculated at 9 km depth than by a centroid depth of 43 km (Figs 3c and d), which is the depth of the inferred subduction interface earthquake in the same region (Example 2), suggesting that this thrust occurred along a splay in the overriding Aegean material. The mechanisms and depths of these two earthquakes, in almost the same place, support the hypothesis that seismogenic splay faults branch from the main subduction zone interface.

3 THE SUBDUCTING AFRICA-NUBIA LITHOSPHERE

As the Africa (Nubia) lithosphere subducts to the north beneath the Aegean, earthquakes within the slab reveal its position to a depth of about 160 km (Fig. 4; Hatzfeld & Martin 1992; Hatzfeld 1994). With a downdip length of 300 km and a present-day convergence rate of 35 mm yr^{-1} between the Aegean and Africa, a seismogenic slab of this length could have been produced in 8.5 Ma, if the convergence rate has been constant. This is less than the observed 10–12 Ma that is typically needed for slabs to heat up enough to become aseismic (e.g. Wortel 1982, 1986), and raises the possibility that the subduction zone itself may only be 8.5 Ma old. However Africa–Eurasia convergence has occurred since at least the Cretaceous (McQuarrie *et al.* 2003) and most of the convergence rate in the Hellenic subduction zone arises from the rapid extension in the Aegean Sea and anticlockwise rotation of Turkey, which may be relatively recent at its present rate (e.g. Angelier *et al.* 1982; Jackson 1994; Armijo *et al.* 1999). A long episode of relatively slow subduction prior to about 3–5 Ma may be responsible for a possible asesimic high-velocity prolongation of the slab penetrating much deeper (to at least 600 km) than the deepest earthquakes (Spakman *et al.* 1998) and widespread andesitic volcanism in the northern Aegean of early Miocene age (Pe-Piper & Piper 2007). The geometry of the seismogenic part of the subducting slab has been reviewed by Hatzfeld & Martin (1992), Hatzfeld (1994) and Papazachos *et al.* (2000), who show that it is relatively flat beneath the Peloponnese, steepening up beneath the Gulf of Corinth, whereas it is more steeply dipping (50°) in the east, near Rhodes (Fig. 4b).

Fig. 4 shows the earthquakes whose depths and locations make it likely they occurred within the subducting lithosphere. Although their focal mechanisms are quite varied, they in fact reveal a relatively simple pattern. Taymaz *et al.* (1990) noted that, south of Crete, the mechanisms of these earthquakes generally had *P*-axes parallel to the local strike of the subduction zone; a pattern seen to be more widespread in the arc by Benetatos *et al.* (2004). In the new enlarged data set it is now clear (Fig. 4c) that this pattern is indeed general round most of the arc, both for earthquakes up to 200 km seaward of the main bathymetric scarp of the Hellenic Trench and to depths of 100 km within the subducting slab itself. There is no evidence for a change in the pattern as the depth increases, and thus no evidence that the slab undergoes a dramatic change in stress state at 50–60 km as claimed by Ganas & Parsons (2009).

The *T*-axes of these earthquakes are, in general, radial to the arc and aligned downdip within the subducting slab (Fig. 4c and Benetatos *et al.* 2004). In some respects this pattern is typical of other subduction zones where the seismically-active slabs do not penetrate as deep as 670 km (Isacks & Molnar 1969; Frohlich 1989), where earthquakes shallower than 410 km generally have downdip *T*-axes. The usual explanation given for this pattern is that the slab is lengthening under its negative buoyancy unless its tip is supported by penetrating to the density contrast at 670 km. In this case it suggests that, even if an older warm and aseismic continuation of the Hellenic slab exists far beyond the deepest earthquakes, it has insufficient strength to influence the earthquake mechanisms at shallow depth.

The along-strike shortening of the downgoing African lithosphere may be related to the strong curvature of the Hellenic subduction zone and its subducting slab. In particular, the consistency of the along-strike *P*-axes and downdip *T*-axes, even as the slab forms itself into a conical surface that increases its curvature with depth, suggests that there is a change in Gaussian curvature that may be related to the seismicity. A surface that changes its Gaussian

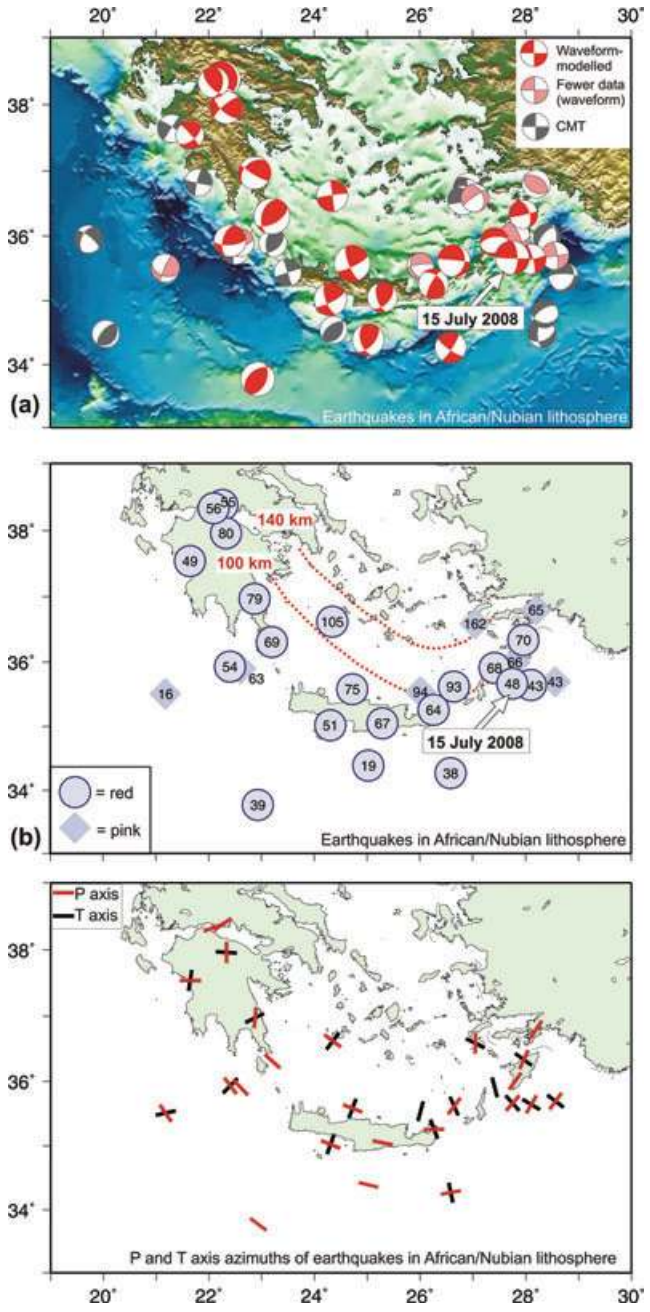

Figure 4. Earthquakes in the downgoing Nubian lithosphere. (a) Focal mechanisms are ranked by quality in the order red, pink, grey (see key and text). The majority are either strike-slip or thrust, and reveal a broad trend of along-arc compression. The location of the event of 2008 July 15, discussed as Example 1 in Fig. 2 is indicated. (b) Well-constrained depths, in km, of waveform-modelled earthquakes [red and pink in (a)]. Depths increase to the north within the subducting slab, which dips more steeply in the east than in the west. Dashed red lines are contours of the slab depth taken from Hatzfeld & Martin (1992). (c) Azimuths of the *P*-axes (red) and *T*-axes (black) with a plunge of less than 45° of earthquakes in (b) show a regular concentric pattern of along-arc shortening, both seaward of the Hellenic Trench and within the subducting slab. *T*-axes are generally radial to the arc, and downdip in the descending slab.

curvature must deform by changing its surface area, which may account for some of the seismicity distribution within the slab. In the case of the Hellenic subduction zone there are too few earthquakes to define the slab geometry over its entire depth range with sufficient precision to test this hypothesis in the manner attempted for the Tonga slab by Nothard *et al.* (1996).

4 AFRICA-AEGEAN CONVERGENCE

Although earthquakes in the subduction zone account for less than 10 per cent of the convergence between Africa and the Aegean, there are sufficient moderate-sized events of M_w 5.0–6.0 to reveal the geometry and depth of the subduction interface in the depth range ∼15–45 km. There are few earthquakes shallower than 15 km (Fig. 5a), probably because of the thick unconsolidated sediment on the downgoing plate and, in common with subduction zones elsewhere, the interface becomes aseismic deeper than ∼45 km because of thermal or dewatering effects (Hyndman *et al.* 1997; Scholz 1998; Stern 2002). In these respects, the Hellenic subduction zone displays a typical distribution of interplate seismicity.

Fig. 6 shows the distribution of thrust and reverse-faulting earthquakes on the subduction zone interface and immediately above it. The epicentres lie in a relatively compact band 50–100 km wide, roughly following the trace of the bathymetric scarps of the Hellenic Trench. The updip continuation of the interface beneath the accretionary prism of the Mediterranean ridge is apparently aseismic. The along-strike distribution of seismicity round the arc is patchy, with dense groups of earthquakes separated by areas without any earthquakes large enough for long period body wave modelling. This irregular distribution is also seen in micro-earthquake studies (Hatzfeld *et al.* 1993; Meier *et al.* 2004). It is unclear whether this patchiness is a long-term feature of the subduction zone, or merely reflects the limited time of observation. It is, however, noteworthy that earthquakes seem to have concentrated in the same areas over three decades; the clusters in Figs 6 and 7 do not represent one main shock and its aftershocks. This may indicate the presence of persistent long-term rough, or well-coupled, frictional patches along the interface (but with relatively small surface areas), surrounded by other areas of stable sliding or creep. The most prominent patches are south of Crete beneath Gavdos, beneath the SW corner of Crete and SW of the Peloponnese.

Low-angle thrust-faulting earthquakes on the subduction interface show some variation in depth with position around the arc (Fig. 6b). In the east, near Rhodes, the only available fault-plane solutions are from first-motion studies, with no precise depth constraints. In this region hypocentral depths from the EHB catalogue, while unlikely to be reliable to better than ∼ ±15 km (Maggi *et al.* 2000b; Engdahl *et al.* 2006), are mostly between 20 and 45 km, which is comparable with other parts of the arc. To the south of Crete, well-determined earthquake depths on the interface occur as deep as 40–45 km, with some shallower events at ∼20 km beneath Gavdos. Beneath the SW corner of Crete, well-determined interface earthquakes are at a depth of 40 km. In western Crete the African Moho, imaged by receiver function studies, is at a depth of 55 km (Li *et al.* 2003), approximately 10 km below the depth of the seismogenic interface, suggesting that the interface follows the top of the subducting oceanic crust. The next substantial patch of earthquakes is south of the Peloponnese, where well-determined depths for low-angle thrusts are typically at 25–30 km. Further west, beneath the Ionian Islands (discussed later), they are shallower still, at 15–20 km. The trend seems to be for the maximum depth of the seismogenic part of the interface to decrease towards the northwest, and this trend seems to correlate broadly with a decrease in sediment thickness in the same direction (Le Pichon *et al.* 1979, 2002; Kastens *et al.* 1992): where the sediment is

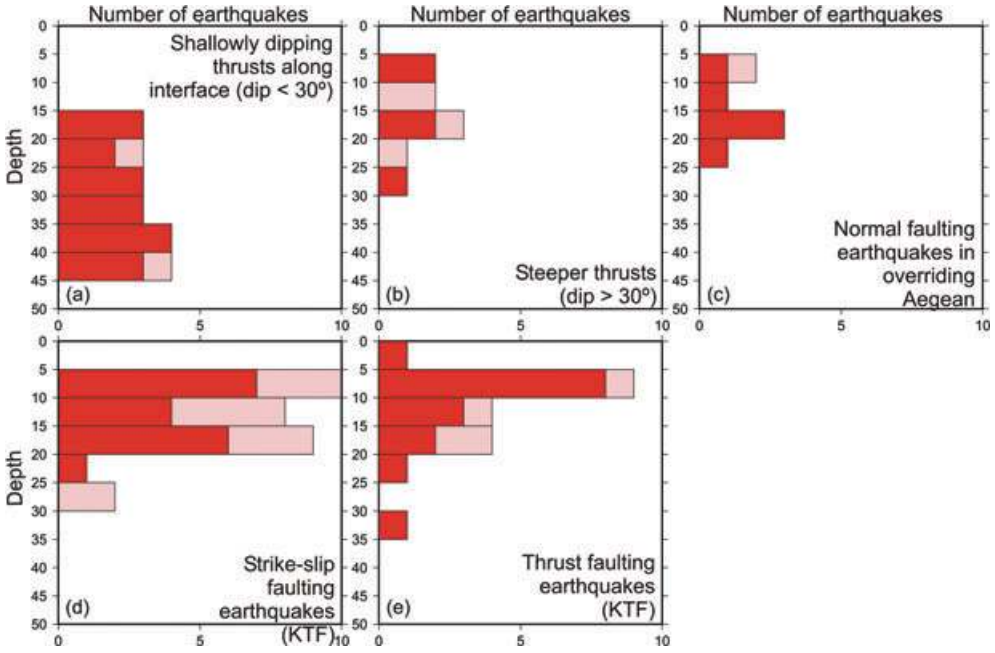

Figure 5. Histograms showing the depth ranges of earthquakes in different tectonic settings. Solid red bars show earthquakes for which there is abundant good quality waveform-modelled data. Pink bars represent earthquakes whose depths are well resolved from waveform modelling, but for which there are insufficient data for the focal mechanism to be determined independently. Shallow-dipping earthquakes along the subduction interface occur at depths between 15 and 45 km. More steeply dipping thrust-faulting earthquakes occur at depths of 5–30 km. Normal-faulting earthquakes in the overriding Aegean material occur between 5 and 25 km. Both strike-slip and thrust-faulting earthquakes in the vicinity of the Kefalonia Transform Fault have similar centroid depths (0–35 km).

thickest the seismogenic part of the interface is deeper, and vice versa.

The mechanisms of the majority of these earthquakes are similar, although the dips of the landward-dipping low-angle fault planes vary between 10 and 20°. For these events, the steep south-dipping auxiliary nodal plane, and therefore the slip-vector, is well constrained as it passes through the centre of the teleseismic station distribution on the focal sphere. The dip of the fault plane itself is less well constrained, but there is a suggestion of a consistent spatial variation, with the shallowest dips (5–10°) in the west of the arc, and steeper dips (approaching 25°) to the south of Crete. The shallower dips in turn are associated with thinner sediment and a shallower depth of interface events.

In addition to shallow-dipping thrust earthquakes along the interface, several reverse-faulting earthquakes with steeper dips (>30°) generally occur at shallower depths than the interface (Fig. 5b), within the overriding material (Fig. 6c). These events presumably occur on splay faults that merge with the interface at depth and accommodate some of the convergence in the subduction zone. Their centroids are typically <20 km depth, whereas low-angle thrusts on the interface in the same regions are deeper, reaching a maximum depth of 40–45 km depth (Fig. 6c). It was one such splay fault beneath SW Crete which Shaw *et al.* (2008) suggested was responsible for the catastrophic AD 365 earthquake and tsunami.

Fig. 7 shows bathymetric and topographic cross-sections through the three main clusters of convergence-related earthquakes in the region of Crete. Each of the cross-sections is plotted so that it runs perpendicular to the local strike of the Hellenic Trench. The first cross-section passes through Western Crete, where the subduction zone interface is at a depth of 40–45 km beneath the Hellenic Trench. In the interpretation of Shaw *et al.* (2008), the earthquake responsible for the 9 m of coastal uplift in AD 365 occurred along a splay fault which reaches the surface at the Hellenic Trench. In their model that best fits the uplift data, the fault extends to 45 km depth, and this bottom of the fault lies directly beneath the northern coast of Crete, suggesting that this splay may be responsible for the position and tilting of Crete itself.

The second cross-section passes through both Gavdos and Crete. There are two clear bathymetric escarpments, both of which may be the surface expressions of splay faults responsible for uplift and tilting. If splays dipping at 30° to a depth of 40 km (dotted red lines) are projected to the surface at the base of these steep escarpments, there is again a reasonable match between the deepest extent of the fault and length scale of tilting for the northern fault in this cross-section.

Cross-section three passes through the earthquakes described in Examples 2 and 3 in Figs 1 and 3. We argue in section 3.5 that the shallower earthquake of 2009 July 1 occurred on a splay fault in the hanging wall of the main subduction zone interface. The surface projection of its north-dipping nodal plane coincides with a clear bathymetric scarp, marked A in Fig. 7(d). Another steep bathymetric escarpment occurs further north (B in Fig. 7d) which could be the surface expression of another north-dipping splay fault. The topography to the north of both these escarpments appears to be tilted N, again on a length scale consistent with the hanging wall of a fault with a 30° dip extending through the entire seismogenic thickness. In both Sections 2 and 3, it is not clear whether the northern inferred splay faults are still active: it may be that the active faulting has migrated south with time.

We can use the pattern of uplift from the AD 365 earthquake as a template to identify sites of possible long-term uplift along the entire straight section of the Hellenic Arc from the south of central Crete to the Ionian Islands (Fig. 8), if points an equal distance from the Hellenic trench are uplifted by an equal amount. If this entire section of the arc behaves in the same way as that suggested for western Crete by Shaw *et al.* (2008), then both the Mani and

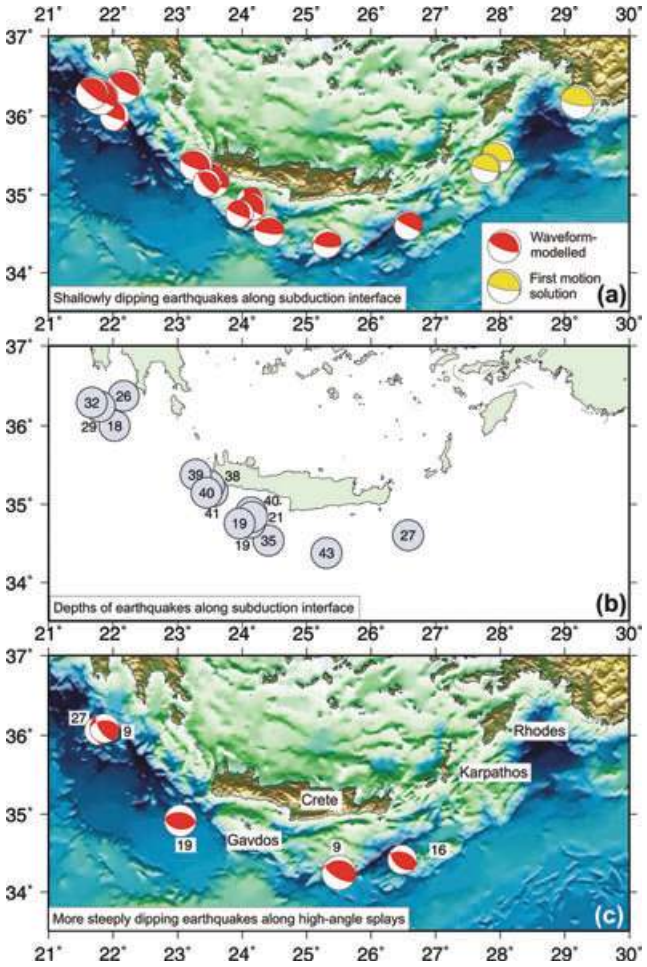

Figure 6. Reliable waveform-modelled fault plane solutions (red), and selected first-motion solutions (yellow) related to Nubia-Aegean convergence. Shallow-dipping thrust faulting earthquakes which occur along the plate interface are plotted in (a) and their depths are shown in (b). More steeply dipping fault plane solutions are plotted in (c). They generally occur at shallower depths than the interface, and probably represent slip along splay faults.

Methoni peninsulae, and possibly Kythera, fall within the expected area of long-term uplift. The Mani peninsula has well-recorded Plio-Quaternary terraces (Kelletat & Gassert 1975; Scheffers *et al.* 2008), and the Methoni peninsula is another obvious place to look for evidence of long-term uplift related to the subduction. Unlike in Western Crete, there is no clear uplifted Holocene shoreline on either of these peninsulae, perhaps suggesting that if they are uplifted in very large earthquakes, such an event has not occurred since sea level stabilized about 6 kyr ago; an argument discussed further by Shaw *et al.* (2008).

The slip-vector azimuths of the thrust and reverse faulting earthquakes in Fig. 6 are shown in Fig. 1(b). Along most of the arc, their direction closely resembles the GPS velocity vectors for the overriding Aegean material relative to Nubia (Fig. 9). In the eastern part of the arc, this similarity in azimuth implies that although the relative motion of the plates is oblique to the bathymetric trenches in this region, the interplate motion is taken up by oblique slip along the subduction zone interface (discussed further in Section 7). Southwest of Crete and the Peloponnese, the match in direction between velocity vectors and slip-vectors is particularly close.

The only significant deviation from this simple picture occurs in the far west of the arc, near the KTF (longitude 20–22°E), where the slip vectors of the thrust earthquakes are almost perpendicular to the GPS vectors (as can be seen in Fig. 13b). This region is discussed separately in Section 8.

Both the GPS velocities and the slip-vectors of earthquakes on the subduction zone interface show a consistent change in azimuth from west to east of about 20°. The divergence in the earthquake slip vectors would require a change in length of about 15 mm yr^{-1} along the arc, assuming a radial convergence of 35 mm yr^{-1} between Nubia and the southern Aegean in the Hellenic Trench system (as shown in Figs 1b and 9), which must be taken up by either extension in the overriding material or shortening in the underthrusting material (or both). The GPS measurements of Hollenstein *et al.* (2008) show 19 mm yr^{-1} extension around the arc, implying that the majority of the divergence seen in the earthquake slip vectors is taken up by extension in the overriding material. This extension is revealed by the earthquakes discussed in the next section.

5 E–W EXTENSION IN THE OVERRIDING AEGEAN

A third important group of earthquakes occurs within the overriding Aegean and is not directly concerned with accommodating Africa-Aegean convergence. These earthquakes represent E–W extension (Fig. 10), mostly on N–S normal faults, and are generally shallower than 20 km (Fig. 5c). Their orientations contrast with the generally E–W striking normal faulting events that characterize the N–S extension of the central and northern Aegean, western Turkey and mainland Greece (McKenzie 1978; Goldsworthy & Jackson 2000).

Although Fig. 10 shows N–S normal faulting earthquakes mainly east and northwest of Crete and in the Peloponnese, normal faults of this trend can be recognised in the topography and bathymetry all round the arc (Lyon-Caen *et al.* 1988; Armijo *et al.* 1992; de Chabalier *et al.* 1992; Huguen *et al.* 2001; Kreemer & Chamot-Rooke 2004). It is likely that the continental crust between the Peloponnese and Crete is below sea level because it has been stretched to a greater extent than the adjacent landmasses. From recent earthquakes, it appears that extension is concentrated in the east and west of the arc, rather than in the centre. The GPS vectors along the arc show the largest divergence in azimuth between 25°E and 29°E longitude, supporting the observation that extension is occurring relatively rapidly in the east of the arc. Several authors (Le Pichon & Angelier 1981; Shaw *et al.* 2008) have suggested that the rapid Quaternary uplift and northward tilting of Crete is caused by the underplating of sediments from the accretionary prism, as they are underthrust beneath Crete on high-angle reverse faults splaying off the subduction interface. As Shaw *et al.* (2008), Stiros & Drakos (2006) and Pirazzoli *et al.* (1996) point out, it is the uplift of Crete that has preserved the evidence which allowed the causative faulting of the AD 365 earthquake to be inferred. If uplift associated with similar underplating between Crete and the Peloponnese has been removed by crustal thinning associated with N–S normal faulting, then so too has any evidence of very large earthquakes of the AD 365 type also been removed from this section of the subduction zone. The potential for such large earthquakes in this part of the zone is consequently not known.

Thus, while it is clear the N–S striking normal-faulting earthquakes seen in western Crete and the Peloponnese by Lyon-Caen *et al.* (1988), Armijo *et al.* (1992) and Taymaz *et al.* (1990) continue

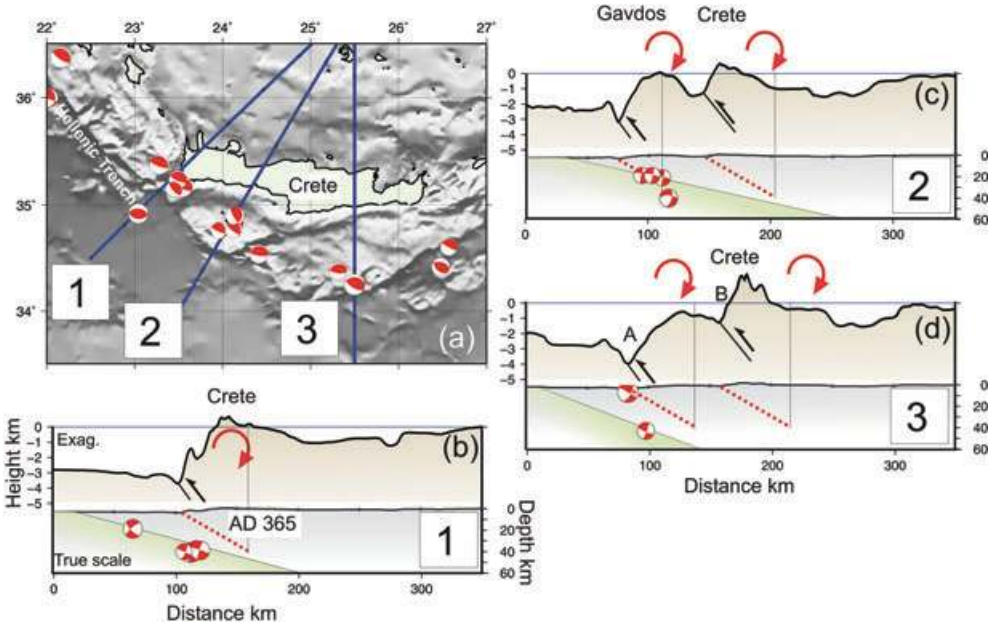

Figure 7. Map (a) and cross-sections (b–d) showing the fault geometry accommodating the main Nubia-Aegean shortening around the Hellenic arc. The three cross-sections pass through clusters of earthquakes around the Hellenic Arc. Cross-section (b) passes through the SW corner of Crete, which was uplifted in the AD 365 earthquake. The lower section is true-scale, whereas the upper section is highly exaggerated in the vertical. A possible geometry for the fault that caused the uplift is plotted as a red dashed line. This fault projects to the surface at the Hellenic Trench, and seems to control both the southern and northern coasts of Crete: the northern coast lies directly above the deepest extent of the fault. The red fault plane solutions are taken from the same subset, with good depth control, that is plotted in Fig. 6. Cross section (c) is east of (a), and shows the possible fault geometry beneath Crete and Gavdos. Cross-section (d) coincides with the location of the 2009 July 1 earthquake (Example 2, Fig. 3).

to the eastern end of the arc, there are no new earthquakes in the west to add to those earlier studies.

6 THE EASTERN TERMINATION

The active tectonics of the eastern end of the subduction zone remains obscure. There are few earthquakes compared with other parts of the arc; some of them have well-constrained focal mechanisms and depths, but many are either within the Nubian lithosphere or related to the E–W extension of the overriding Aegean. In Fig. 11, we show the earthquakes whose mechanisms and depths suggest they could reflect some part of the primary Nubia-Aegean motion across the zone. The earthquakes do not line up to reveal a major fault, but do indicate two main types of faulting:

(1) The first are thrust-faulting earthquakes with a shallow northward dip (Fig. 11a), whose slip vectors closely parallel the GPS vectors. They are capable of taking up the motion between Nubia and the Aegean on the subduction zone interface. These earthquakes may be associated with hummocky E–W ridges perpendicular to their slip vectors (Figs 11a and c).

(2) The second type are compatible with NE–SW left-lateral strike-slip faulting (Fig. 11b), with slip vectors in the range SSW–WSW. The strike of the fault-planes and of their slip-vectors are sometimes parallel to local bathymetric lineations (Fig. 11c) which may represent multiple strike-slip faults.

A type of faulting that is conspicuously absent is thrusting with a strike parallel to the NE–SW deforming zone and an orthogonal (i.e. SE) slip vector. Thus there is no evidence for the classic form of slip partitioning common in subduction zones (Fitch 1970; McCaffrey 1996). Instead, the whole region is distinctly broken-up, with hummocky topography that may represent the surface expression of thrust faults and some more linear features that may represent strike-slip faults. This deformation is distributed in the overriding material, which must be underlain by a relatively shallow north-dipping interface, as seismicity in the Nubian slab continues to a depth of over 100 km (Fig. 4b, Hatzfeld & Martin 1992). The distributed strike-slip faulting, with slip vectors oblique to those on the thrusts, is a style of deformation familiar from Mongolia (Bayasgalan *et al.* 1999) and Iran (Walker *et al.* 2003), which can contribute to the NNE–SSW convergence if the strike-slip faults rotate clockwise with time. In Mongolia and Iran the rotating strike-slip faults often terminate in thrusts: south of Rhodes and Karpathos, this may be the origin of the hummocky ridges. The analogous behaviour in an extensional setting is seen in central Greece, where strike-slip faults end in extensional graben (Goldsworthy *et al.* 2002).

7 THE WESTERN TERMINATION

7.1 Strike-slip faulting

An abrupt bathymetric escarpment, around 4 km deep, and sometimes called the KTF (Kokinou *et al.* 2006), runs along the NW edge of the Ionian Islands, and forms the western termination of the Hellenic subduction zone. It is associated with a high level of seismicity, much of it compatible with NE–SW right-lateral strike-slip faulting (Baker *et al.* 1997). Louvari *et al.* (1999) suggested it consisted of two segments with different strikes: a southern segment 90 km long that strikes NE, and a northern segment 40 km long striking NNE. There is some support for these two different segments in the different slip vectors north and south of Kefalonia in Fig. 12(b).

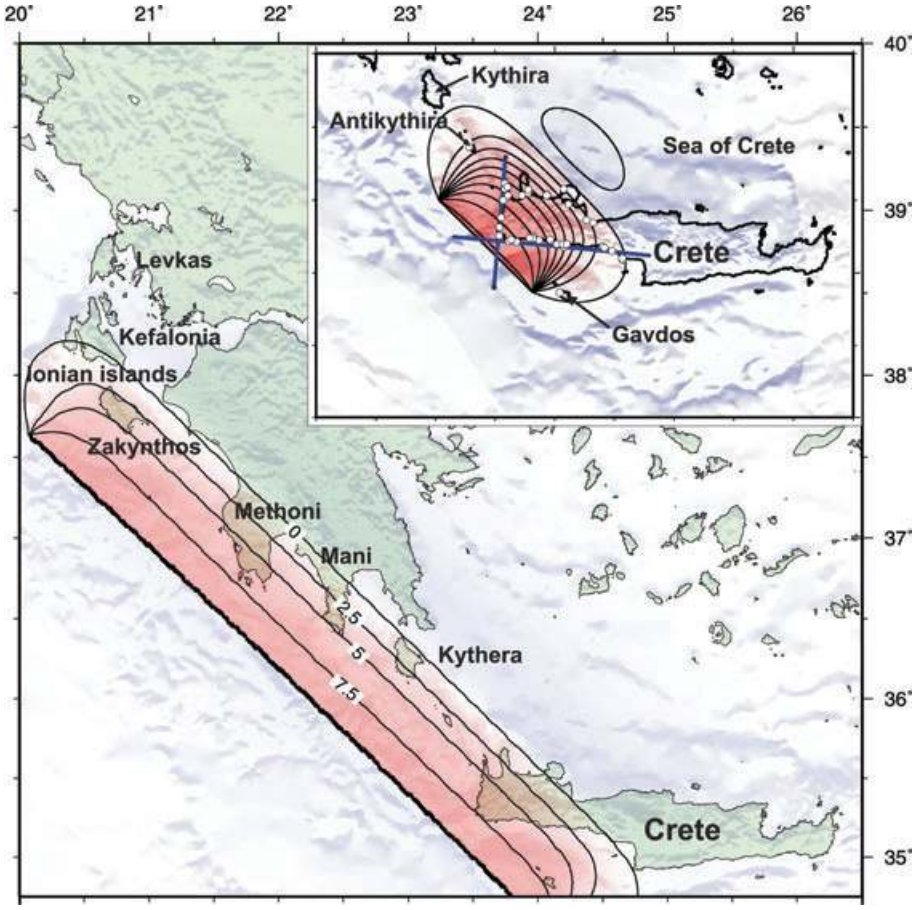

Figure 8. Inset shows the inferred uplift distribution during the AD 365 earthquake on Crete from Shaw *et al.* (2008) based on an elastic dislocation model and constrained by observations at the circled locations. Contours are at metre intervals, with a maximum of 9 m uplift. The main figure shows this uplift distribution extrapolated along strike, with contours of uplift at intervals of 2.5 m. If this section of the Hellenic Trench experiences earthquakes similar to that of AD 365, then this pattern may be used to predict areas that may be uplifted in the long term, such as the Mani and Methoni peninsulae, and the island of Kythera. The maximum uplift is the same in the main figure and the inset.

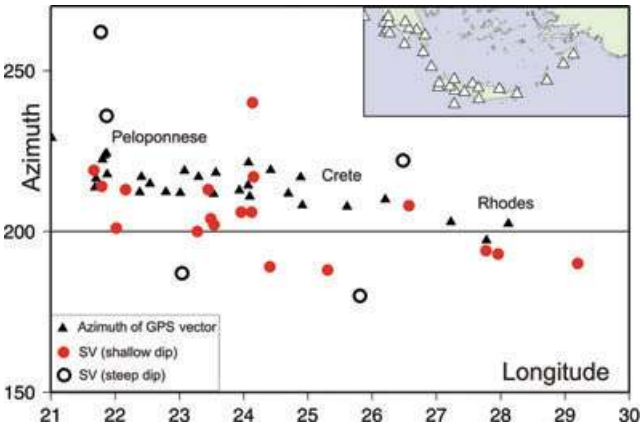

Figure 9. The variation in the azimuths of GPS velocities relative to Nubia (triangles) and earthquake slip-vectors (circles) around the Hellenic arc. The red circles are slip vectors of shallowly dipping earthquakes along the subduction-zone interface; open circles represent the slip-vectors of more steeply dipping thrust-faulting earthquakes at shallower depths in the overriding material. The GPS vectors and slip-vectors show a consistent divergence of just under 20 mm yr^{-1} between the west and east of the arc. The inset shows the positions of the GPS stations whose velocity vectors are plotted in the main panel.

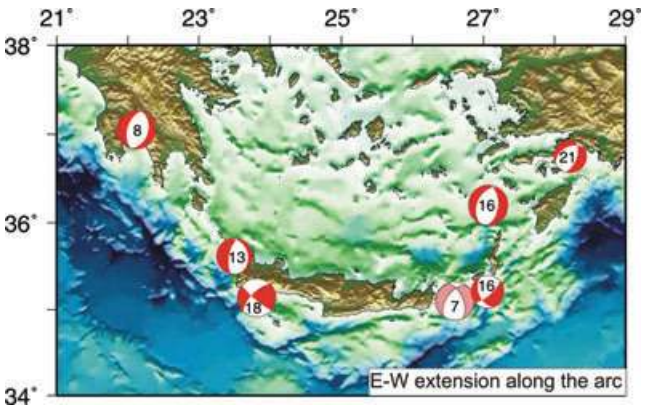

Figure 10. Earthquakes indicating E–W extension in the overriding Aegean material above the subduction-zone interface. Centroid depths (in km) are plotted in the focal mechanisms. The highest-quality waveform-modelled solutions are in red; those in pink have also been modelled, but with fewer data. The E–W extension represented by these earthquakes has been concentrated in the east and west of the arc, rather than in the centre, over the period of observation.

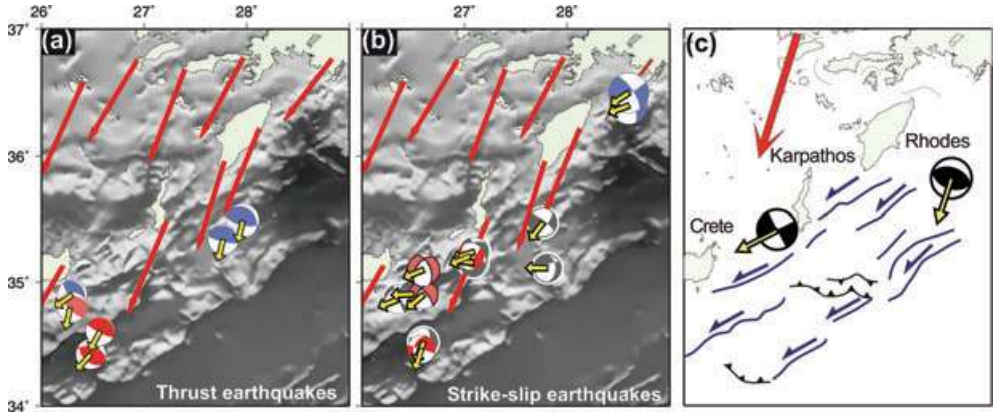

Figure 11. Earthquakes at the eastern end of the Hellenic arc that contribute to the main Nubia-Aegean convergence. Focal spheres are coloured by quality as in Fig. 4, with the addition of first-motion solutions, which are plotted in blue. (a) Thrust faulting earthquakes have slip vectors (yellow) subparallel to the GPS velocities (red). (b) Strike-slip faulting earthquakes have slip vectors oblqiue to the GPS velocities, but their strikes align with bathymetric lineations. (c) An interpretive summary, showing strike-slip fault strands as blue lines and the hummocky surface expression of blind thrusts as black lines.

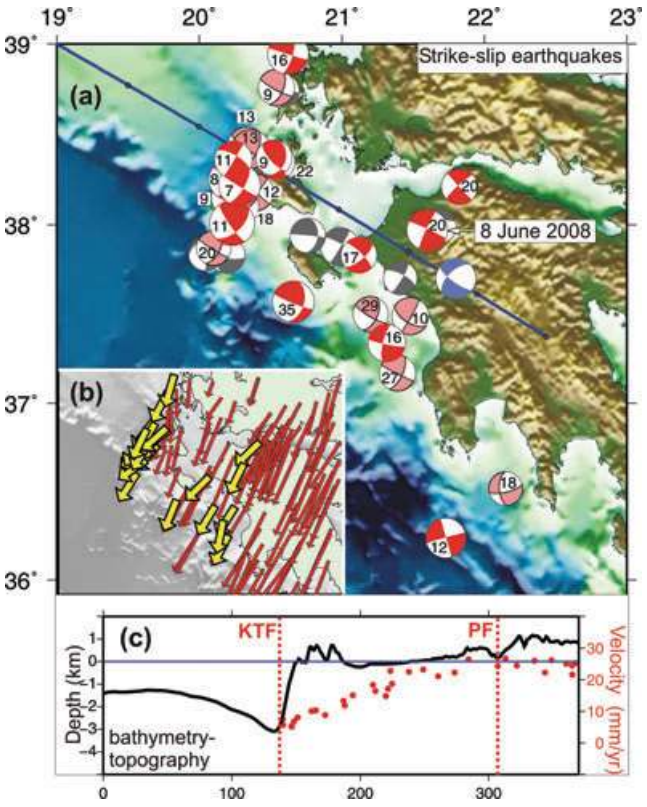

Figure 12. Strike-slip faulting earthquakes at the western termination of the subduction zone. Well-determined depths are given as numbers adjacent to the focal mechanisms. The colour of the focal mechanism denotes its method of determination and the quality of the data, as in Figs. 4 and 11. The blue line running from NW to SE is the line of cross-section in (c). The inset (b) shows the slip vectors of the waveform-modelled earthquakes (yellow) and the GPS velocities relative to Nubia (red). The cross-section (c) shows the bathymetry-topography (black line) along the section, alongside the trench-perpendicular component of the GPS velocities (red dots). The magnitude of the GPS velocities gradually increases between the Kefalonia transform fault (KTF) and the Patras fault (PF), revealing a region of distributed shear that is consistent with the spread of earthquake focal mechanisms.

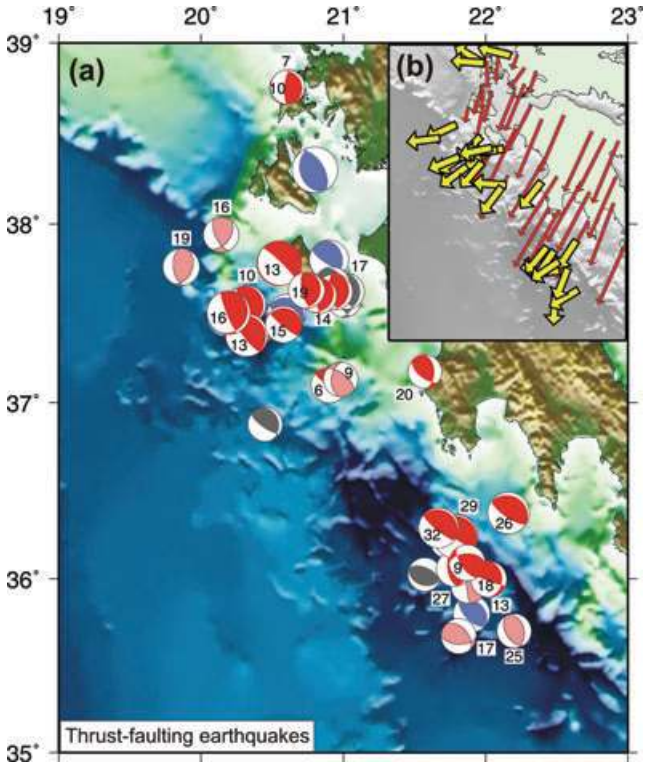

Figure 13. Thrust faulting earthquakes at the western termination of the subduction zone. Well-determined depths are given as numbers adjacent to the focal mechanisms. The colour of the focal mechanism denotes its method of determination and the quality of the data, as in Fig. 12. The inset shows the slip vectors of the waveform-modelled earthquakes (yellow) and the GPS velocities relative to Nubia (red).

In addition to earthquakes along the two segments of the Kefalonia Transform Fault, Louvari *et al.* (1999) recognised a few strike-slip earthquakes which did not occur along this prominent bathymetric escarpment, but were further to the SE. A recent strike-slip earthquake of M_w 6.3 on 2008 June 8 in the NW Peloponnese, close to the city of Patras (Fig. 12), belonged to this group. Its aftershocks defined a zone running NE–SW along a line separating mountainous topography to the SE from the gently undulating,

broad coastal plain to the NW (Ganas *et al.* 2009; Konstantinou *et al.* 2009). The focal mechanism is well determined by waveform modelling and indicates NE–SW right-lateral strike-slip faulting with an unusually deep centroid at 20 km. From its seismic moment, the estimated source dimension is of order 10–15 km, explaining the lack of a continuous coseismic surface rupture.

The NE–SW right-lateral shear that crosses central Greece (McKenzie 1972) and is seen clearly in the GPS velocity field (Fig. 1b; Reilinger *et al.* 2006) is accommodated mostly by clockwise rotations of normal faults and the blocks they bound about a vertical axis (McKenzie & Jackson 1983; Goldsworthy *et al.* 2002; Mattei *et al.* 2004). At the western termination of the subduction zone, it is instead accommodated by NE–SW right-lateral strike-slip faulting, which includes the KTF but is also distributed over a zone ∼100 km wide to the SE. The slip-vectors of strike-slip faulting earthquakes are almost parallel to the GPS vectors in this region (Fig. 12b). The distributed strike-slip motion is seen both in the focal mechanisms (Fig. 12a) and the steady gradient in GPS velocities (Figs 12b). Fig. 12(c) is a cross-section through the topography and bathymetry in a direction perpendicular to the KTF (blue line). The magnitude of the SW component of the GPS velocities is plotted in red, and reveals a gradual SE-ward increase in SW-directed velocity from nearly zero to the northwest of Kefalonia, to ∼30 mm yr^{-1}, close to the total Aegean-Nubian convergence, to the south-east of the Patras Fault (PF), recognized from GPS and seismicity. It is clear that there is not a single dextral strike-slip fault, but rather several strands accommodating the motion, similar to the situation in the North Aegean, where the North Anatolian fault also branches into several strands (Taymaz *et al.* 1991).

7.2 Thrust faulting earthquakes

To the south of the Peleponnese, the thrust faulting earthquakes are typical of those interface events seen elsewhere around the arc (Fig. 13). The earthquakes along the interface occur at depths of 20–25 km, and are on shallowly dipping thrust faults. However, beneath the Ionian Islands (Kefalonia, Zakynthos and Levkas) the thrust faulting earthquakes have a different character: their strike is N–S, and their slip vectors are almost perpendicular to the GPS convergence direction (Fig 13b), suggesting a degree of slip partitioning in this region.

Figs 5(d) and (e) show histograms of the depths of strike-slip and thrusting earthquakes near the western termination. Here the subduction zone interface is relatively shallow, so almost all of the earthquakes are shallower than 20 km depth. Both the thrust and strike-slip earthquakes have a similar depth distribution.

7.3 Gravity and flexure

NW of the KTF, the bathymetry deepens and the negative free-air gravity anomaly increases towards the SE, resembling a flexural signal. Using the technique described in detail by McKenzie (2003), NE–SW gravity and topography profiles were stacked within the box outlined in red in Fig. 14 and the resultant profiles matched by the flexure of an elastic beam with thickness T_e. Consistent values for T_e of 7–8 km (±1.5 km) were obtained either from the gravity or the topography (Fig. 14) though the plots of misfit against T_e are broad and do not have well-determined minima. These values of T_e are similar to those estimated for Italy using the admittance method of gravity and topography by D'Agostino & McKenzie (2002). Such low values are typical of young continental regions (Maggi *et al.* 2000a), and suggest that the area NW of Kefalonia, that is, the S Adriatic, is indeed continental, and that the change in water depths and earthquake centroid depths north of 40°N marks the transition from the subduction of oceanic lithosphere to the *S* to continent–continent collision in NW Greece.

The KTF juxtaposes high-topography (Ionian Islands) with the deeper seafloor of the Ionian Sea. Much of this relief is probably inherited by the SW motion of the Ionian Islands on the KTF, and some may be enhanced by the thrusting of the Ionian Islands to the west causing the Ionian Sea to flex in response (Fig. 15). The GPS velocity vectors do not show any significant movement of the Ionian Islands normal to the Kefalonia Transform fault, but the islands would act as a load regardless of how they were emplaced (i.e. whatever the relative direction of motion between the Ionian Islands and the Southern Adriatic). The agreement between GPS velocities and slip vectors on the strike-slip faults shows that the loading is principally by emplacement along a lateral ramp, perpendicular to the main thrust front in the SW. The flexural loading is presumably more obvious at the western termination of the arc (i.e. west of Kefalonia) than south of the Peloponnese because of the thick sediments in the south. The N–S striking thrust faulting earthquakes may be related to the collapse of the overthrust material in the east along the steep bathymetric escarpment of the Kefalonia Transform Fault.

8 THE CONNECTION WITH THE AEGEAN AND CENTRAL GREECE

The abundant data from earthquake focal mechanisms, slip vectors and GPS velocities reveal how faulting accommodates the large-scale motions of the Aegean and Eastern Mediterranean. The most obvious features of the GPS velocity field are the flow of Aegean material towards the SW (Fig. 1b), the relative rigidity of the southern Aegean, and the shear between Europe and Turkey, which continues through the North Aegean into central Greece (McClusky 2000; Hollenstein *et al.* 2008; Reilinger *et al.* 2009). Earthquakes in the Eastern Mediterranean closely reflect this velocity field: shallowly dipping thrust earthquakes along the plate interface reveal the convergence between the Aegean and Nubia; the southern Aegean is largely aseismic (Jackson 1994); and strike-slip earthquakes align in strands through the North Aegean (Goldsworthy *et al.* 2002).

Where the NE–SW right-lateral strike-slip fault branches in the north Aegean reach the eastern coast of Central Greece, they connect to the rapidly opening gulfs of Volos and Evia (Goldsworthy *et al.* 2002), which are opening fastest in the east (Clarke *et al.* 1998; Briole *et al.* 2000; Avallone *et al.* 2004). Yet the most seismically active and rapidly opening graben system in this region is the Gulf of Corinth, which opens fastest at its western end, where it appears to connect with the strike-slip fault system on which the 2008 Patras earthquake occurred. Similarly, the KTF projects to the western end of the Gulf of Arta which appears to be another normal-faulted basin, like other graben on the west coast, such as the Trichonis basin (Goldsworthy *et al.* 2002; Kiratzi *et al.* 2008). As the slip vectors on all the E–W normal faults are roughly N–S (Goldsworthy *et al.* 2002) whereas the overall motions are to the SW, the blocks between the normal faults must rotate about vertical axes (McKenzie & Jackson 1983). It is this block rotation, confirmed in places by palaeomagnetic measurements (Mattei *et al.* 2004), that accommodates shear in central Greece. Thus the connection to strike-slip faults on the western side of Central Greece, along the KTF, Patras Fault and other parallel faults in some ways resembles that on the eastern side of this system, in the Aegean. Fig. 16 is a cartoon showing our interpretation of the region. Central Greece is sheared in a

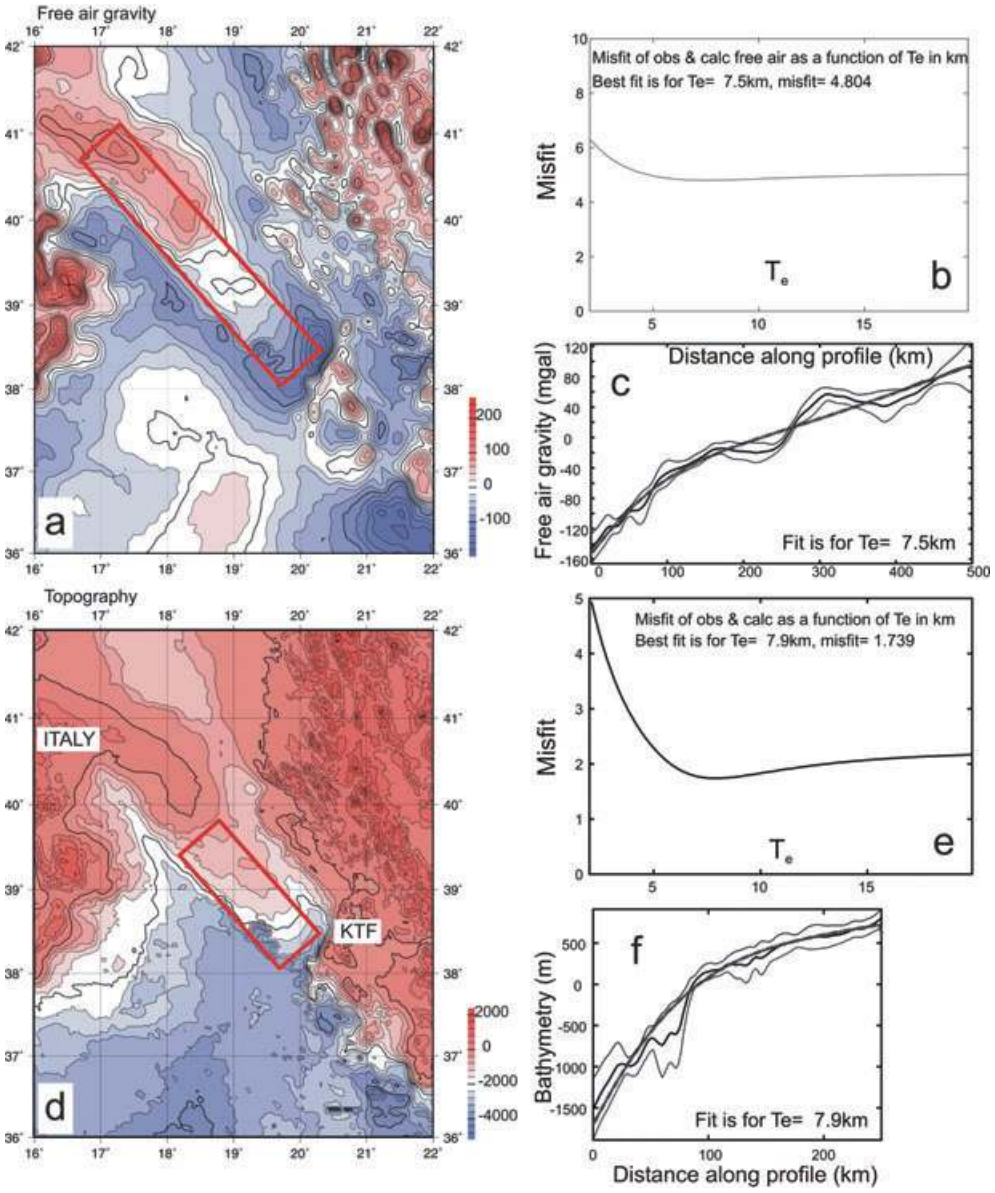

Figure 14. (a) Free-air gravity map for the Southern Adriatic (Sandwell & Smith 2009). Profiles within the red box were stacked and then modelled by a flexed elastic beam to estimate the effective elastic thickness (T_e), following the procedure of McKenzie (2003). In (b) the resulting misfit between observed and calculated free air gravity is plotted against T_e, showing a broad, poorly resolved minimum, with a formal best fit for a T_e value of 7.5 km. (c) shows the stacked gravity profiles against distance along the profile (in km), with a 1σ error envelope. The thick dashed line shows the best-fitting solution. (d) is a map of topography (Smith & Sandwell 1997) in the region. Profiles within the red box were stacked and then also modelled as a flexed beam to estimate T_e. Panel (e) shows the resulting misfit between observed and calculated topography as a function of T_e. In this case the minimum, though broad, is clearer, and the best fitting solution for T_e is 7.9 km, consistent with the result obtained from the gravity modelling. (f) shows the stacked profiles against distance along the profile (in km), with a 1 σ error envelope. The thick dashed line shows the best-fitting solution.

right-lateral sense. The whole region accommodates a gradient in SW-directed velocity, relative to the north (Fig. 1). In the east, this shear is taken up by strike-slip faulting which ends in normal-faulted graben that open most rapidly in the east. In the west, another set of graben open fastest at their western ends, connecting to a second set of strike-slip faults in the Ionian Islands and W. Peleponnese. The areas between the normal faults rotate clockwise relative to the north, which is why the slip-vectors on the normal faults are N–S, not NE–SW. Thus the graben of Central Greece act as a regional relay zone, connecting two strike-slip faulting systems in the NE and SW. In reality, the blocks are not entirely rigid, and there are many minor faults at the ends of the major faults. The simplified cartoon of Fig. 17 considers only the major active faults in the region, and only their relation to the present-day earthquakes and GPS motions. The earlier geologic history of the Gulf of Corinth may well have been more complicated (e.g. Bell *et al.* 2009).

Fig. 17 is a cartoon summarising the main tectonic features of the Hellenic subduction zone between NW Greece and Central Crete, integrating the insights of Goldsworthy *et al.* (2002) in the northern part of the area with those of this study. The African slab subducts to the North, undergoing along-arc compression as it descends in to the arcuate subduction zone, accompanied by along-arc extension in the overriding Aegean. In the cross-section, Santorini marks the position of the volcanic arc (shown as a triangle in Fig. 17). The

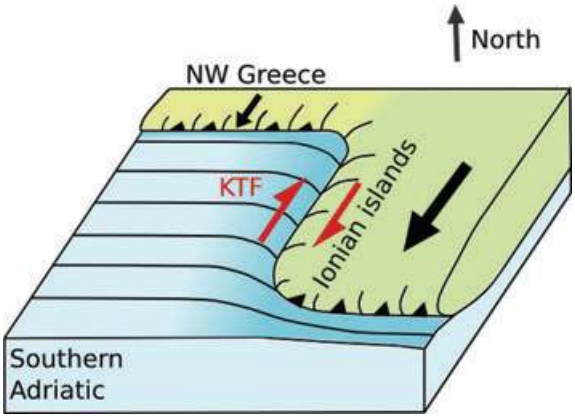

Figure 15. Interpretation of the kinematics in the area of the Kefalonia Transform Fault. The Southern Adriatic is underthrust beneath NW Greece along a line of shallowly dipping thrust faulting earthquakes that run along the coastline (Baker *et al.* 1997; Copley *et al.* 2009). The Ionian Islands and the Peleponnese are thrust to the SW, at a rate of up to 35 mm yr^{-1}, overriding the oceanic lithosphere of the Ionian Sea. The Ionian Islands act as a load on the Southern Adriatic, emplaced along a lateral ramp, and the Southern Adriatic flexes in response. Shear between the Ionian Islands and the Southern Adriatic is accommodated along the Kefalonia Transform Fault (KTF).

Nubian lithosphere is covered in a thick pile of sediments, and the Aegean overrides these sediments along splay faults, leading to uplift of Crete. Shear between the Aegean and Eurasia is taken up by strike-slip faulting in the Aegean and in the region of the Ionian Islands, but is accommodated by block rotation and normal faulting in Central Greece.

9 CONCLUSIONS

The aim of this study was to use earthquake source parameters and GPS data to elucidate kinematic features of the Hellenic subduction zone. The principal new results of this study are:

(1) We have shown that careful re-evaluation of earthquake focal mechanisms and depths, and their comparison with the now excellent GPS velocity data, allows the seismcity and deformation within the subducting Nubian lithosphere, the overriding Aegean lithosphere, and on the interface between them, to be distinguished; a result previously demonstrated only near Crete (Taymaz *et al.* 1990).

(2) We confirm that deformation nearly everywhere within the Nubian lithosphere is characterized by concentric along-arc shortening, mostly by reverse and strike-slip faulting, and show that it is seen in earthquakes as far as 200 km seaward of Crete and to depths of at least 100 km north of Crete. The ubiquity of this pattern suggests it is related to the strong along-strike curvature of the subduction zone.

(3) Earthquakes on the subduction interface itself are low-angle thrusts in the depth range 15–45 km, generally reaching a maximum depth of 20 km in the west and 45 km in the centre of the arc, near Crete. Shallower steeper-dipping reverse faults occur above the main interface in most parts of the arc, and probably occur on splay faults connecting with the subduction interface at depth.

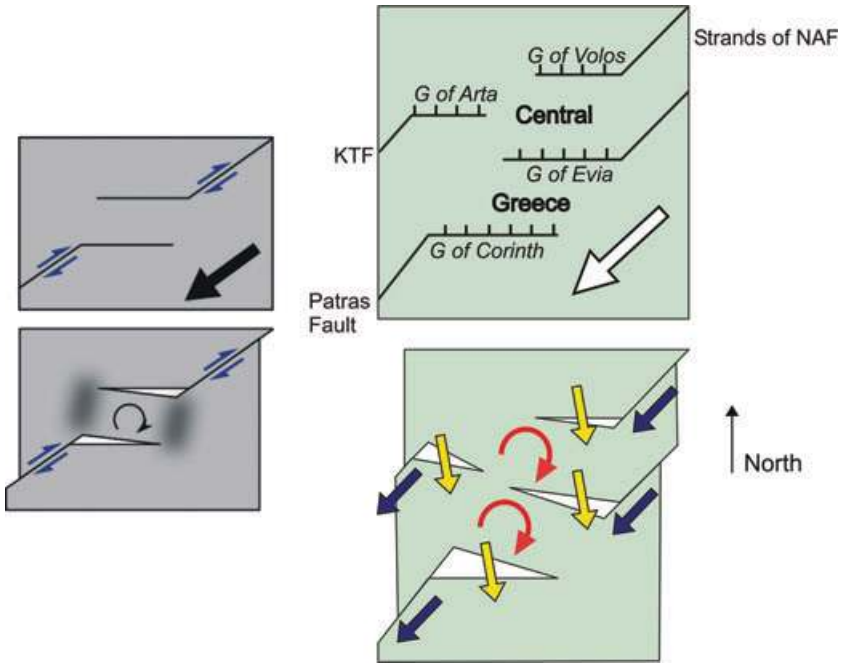

Figure 16. Cartoon showing the kinematics of Central Greece, modified from Goldsworthy *et al.* (2002). For locations, see Fig. 1. On the left is a simple case, in which right-lateral shear is transferred through a region by extensional faulting and block rotation. When motion occurs along the strike-slip faults, the central block rotates, and diffuse deformation is expected at the edges of this block (shaded region in bottom panel). The panels on the right show how this simple concept can be applied to Central Greece. Rather than a single strike-slip fault offset by a normal faulting system, parallel strike-slip faults connect with graben and the blocks between these graben rotate. In the east, several strands of the North Anatolian Fault (NAF) connect to graben which open most rapidly at their eastern ends (Volos and Evia). In the west, the graben open most rapidly at their western ends, and connect to the Kefalonia and Patras transform faults. This panel shows how strike-slip faults terminate in normal-faulted graben, which accommodate the shear by rotations (red arrows). The strike-slip faulting earthquakes have slip vectors (blue) which are parallel to the direction of shearing, whereas the slip-vectors of normal-faulting earthquakes are N–S. The blocks between the normal-faulted graben will rotate clockwise. Note that the structural expression of rotations is in graben whose extension varies rapidly along strike.

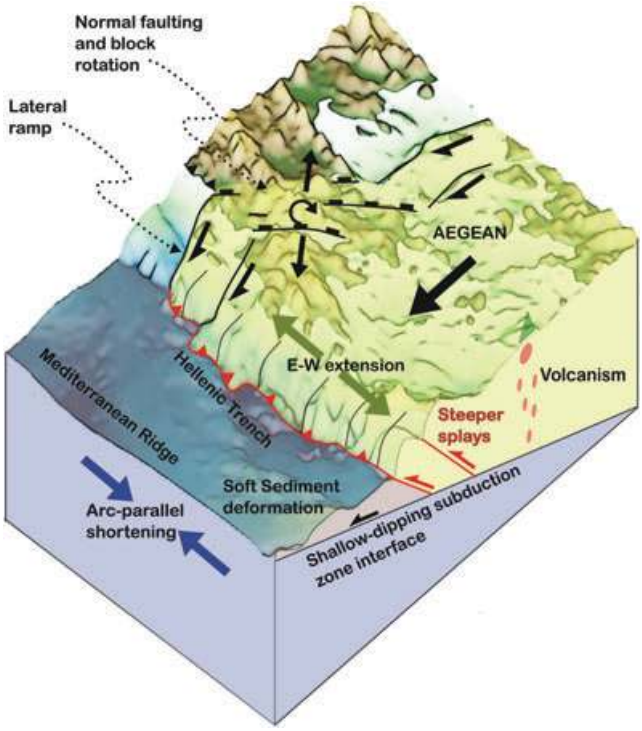

Figure 17. Cartoon summarising the main tectonic features of the Hellenic subduction zone, between NW Greece and Crete. The descending Nubian lithosphere is shown in blue, overlain by a thick accretionary prism (grey) which forms the Mediterranean Ridge. As the Nubian lithosphere enters the arcuate subduction zone, it contracts in an arc-parallel direction. The overriding Aegean is shown as yellow, and deforms by arc-parallel extension along N–S normal faults. The Hellenic Trench marks the position of a splay fault, along which Aegean material overthrusts the accretionary prism, causing uplift. The Aegean is moving SW with respect to Eurasia, and this relative motion is taken up by strike-slip faults in the Aegean and Ionian Islands. Between these strike-slip faulting systems, Central Greece deforms by normal faulting and block rotation, acting as a regional relay zone. Apulia is flexed beneath the Ionian islands due to a lateral ramp (see Fig. 15).

(4) With the depth extent and dip of the seismogenic part of the main subduction interface well defined, we confirm that, even allowing for the contribution of small earthquakes and the occasional very large AD 365-type event, the main subduction zone interface must be largely uncoupled and aseismic. The principal large earthquake and tsunami hazard is likely to be from rare AD 365-type events on splay faults, as described by Shaw *et al.* (2008).

(5) The close agreement between GPS velocities relative to Nubia and earthquake slip vectors on the subduction interface, both of which are radial to the arc in the centre and west, requires an along-arc change in length. Most of this is probably achieved by along-strike extension of the overriding arc.

(6) In the west, the subduction zone terminates in a steep bathymetric escarpment that is predominantly a strike-slip fault (the KTF; e.g. Baker *et al.* 1997), which also marks a change from oceanic subduction to continent–continent collision. Earthquake mechanisms, GPS data and a flexural gravity anomaly show that the origin of the escarpment is as a lateral ramp, formed as the Ionian Islands are emplaced SW onto the Apulian lithosphere. Some thrust faulting with slip vectors perpendicular to the ramp reveal an element of slip partitioning in the region, which enhances the relief of the scarp.

(7) GPS data and strike-slip earthquake mechanisms show that NE–SW right-lateral shear at the western end of the subduction zone is not restricted to the KTF, but is distributed on several parallel strike-slip faults over a distance of ∼150 km. One of these was responsible for the destructive earthquake of 2008 June 8 near Patras.

(8) At the eastern end of the subduction zone low-angle thrust faults with slip vectors oblique to the strike of the arc, but parallel to the Nubia-Aegean convergence measured by GPS, occur on the main subduction zone interface. The interface is overriden by material that is pervasively deformed by distributed strike-slip faults responsible for linear escarpments, and hummocky bathymetry that may be associated with blind splay thrusts. Slip vectors on the strike-slip faults are oblique to those on the thrusts and to the Nubia-Aegean convergence, suggesting that the strike-slip faults rotate about vertical axes.

(9) The GPS velocity field in Greece shows a 150–200 km wide band of NE–SW right-lateral shear extending from the NE Aegean to the SW termination of the Hellenic subduction zone (e.g. McKenzie & Jackson 1983; McClusky 2000). In the NE and SW this motion is achieved by parallel NE–SW strike-slip faults. In central Greece it is achieved by clockwise-rotating blocks bounded by E–W normal faults with N–S slip vectors. In both the east and west of central Greece, the strike-slip faults terminate in graben that die out towards the centre of Greece. The rapid gradients of extension along-strike of these graben is the structural manifestation of the clockwise rotation. Central Greece thus acts as a relay zone connecting the strike-slip faults to either side.

ACKNOWLEDGMENTS

We are greatly indebted to M. Floyd, P. England and J-M. Nocquet, who provided the combined cGPS velocity field that was used extensively in this paper. We are extremely grateful to Dan McKenzie, for the estimates of elastic thickess that he provided, as well as his suggested improvements to the manuscript. R. Engdahl kindly made available updated versions of the catalogue of Engdahl *et al.* (1998). We thank Gavin Hayes and an anonymous reviewer for particularly detailed comments that improved this paper. This work was supported by COMET+, within the Dynamic Earth and Natural Hazards theme of the National Centre for Earth Observations, funded by the Natural Environmental Research Council.

REFERENCES

Altamimi, Z., Collilieux, X., Legrand, J., Garayt, B. & Boucher, C., 2007. ITRF2005: a new release of the International Terrestrial Reference Frame based on time series of station positions and Earth Orientation Parameters, *J. geophys. Res.,* **112,** B09401.

Ambraseys, N.N., 1962. Data for the investigation of the seismic sea-waves in the Eastern Mediterranean, *Bull. seism. Soc. Am.,* **52,** 895–913.

Ambraseys, N.N., 1978. The relocation estimatedof epicentres in Iran, *Geophys. J. R. astr. Soc.,* **53,** 117–121.

Ambraseys, N.N., 2009. *Earthquakes in the Mediterranean and Middle East*, Cambridge University Press, Cambridge.

Ambraseys, N.N., Melville, C.P. & Adams, R.D., 1995. *The Seismicity of Egypt, Arabia and the Red Sea: A Historical Review.* Cambridge University Press, Cambridge.

Angelier, J., Lyberis, N., Le Pichon, X. & Huchon, P., 1982. The tectonic development of the Hellenic Trench and Sea of Crete: a synthesis, *Tectonophysics,* **86,** 159–196.

Armijo, R., H., Lyon-Caen, and Papanastassiou, D., 1992. East-west extension and Holocene normal fault scarps in the Hellenic arc, *Geology,* **20,** 491–494.

Armijo, R., Meyer, B., Hubert, A. & Barka, A., 1999. Westward propagation of the north anatolian fault into the northern aegean: timing and kinematics, *Geology,* **27,** 267–270.

Avallone, A. *et al.*, 2004. Analysis of eleven years of deformation measured by GPS in the Corinth Rift Laboratory area, *Comptes Rendus Geosci.,* **336,** 301–311.

Baker, C., Hatzfeld, D., Lyon-Caen, H., Papadimitriou, E. & Rigo, A., 1997. Earthquake mechanisms of the Adriatic Sea and Western Greece: implications for the oceanic subduction-continental collision transition, *Geophys. J. Int.,* **131,** 599–594.

Bayasgalan, A., Jackson, J., Ritz, J.-F. & Carretier, S., 1999. Field examples of strike-slip fault terminations in Mongolia and their tectonic significance, *Tectonics,* **18,** 394–411.

Bell, R.E., McNeill, L.C., Bull, J.M., Henstock, T.J., Collier, R.E.L. & Leeder, M.R., 2009. Fault architecture, basin structure and evolution of the Gulf of Corinth Rift central Greece, *Basin Res.,* **21,** 824–855.

Benetatos, C., Kiratzi, A., Papazachos, C. & Karakaisis, G., 2004. Focal mechanisms of shallow and intermediate depth earthquakes along the Hellenic Arc, *J. Geodyn.,* **37**(2), 253–296.

Berberian, M., 1979. Evaluatiuon of the instrumental and relocated epicentres of Iranian earthquakes, *Geophys. J. R. astr. Soc.,* **58,** 625–630.

Bohnhoff, M., Makris, J., Papanikolaou, D. & Stavrakakis, G., 2001. Crustal investigation of the Hellenic subduction zone using wide aperture seismic data, *Tectonophysics,* **343,** 239–262.

Briole, P. *et al.*, 2000. Active deformation of the Corinth rift, Greece: results from repeated global positioning system surveys between 1990 and 1995, *J. geophys. Res.,* **105,** 25 605–25 625.

Camerlenghi, A., Cita, M.B., Hieke, W. & Ricchiuto, T., 1992. Geological evidence for mud diapirism on the Mediterranean Ridge accretionary complex, *Earth planet. Sci. Lett.,* **109,** 493–504.

Chaumillon, E. & Mascle, J., 1995. Variations laterales des fronts de deformation de la Ride Mediterraneene, *Bulletin de la Societe Geologique de France,* **166,** 463–478.

Chaumillon, E. & Mascle, J., 1997. From foreland to forearc domains: new multichannel seismic reflection survey of the Mediterranean Ridge accretionary complex (Eastern Mediterranean), *Mar. Geol.,* **138,** 237–259.

Clarke, P.J. *et al.*, 1998. Crustal strain in central Greece from repeated GPS measurements in the interval 1989–1997, *Geophys. J. Int.,* **135,** 195–214.

CMT, 2009. Global cmt project: http://www.globalcmt.org.

Copley, A., Boait, F., Hollingsworth, J., Jackson, J. & McKenzie, D., 2009. Subparallel thrust and normal faulting in Albania and the roles of gravitational potential energy and rheology contrasts in mountain belts, *J. geophys. Res.,* **114,** B05407, doi:10.1029/2008JB005931.

Cowie, P.A. & Scholz, C.H., 1992. Displacement-length scaling relationship for faults: data synthesis and discussion, *J. Struct. Geol.,* **14,** 1149–1156.

D'Agostino, N. & McKenzie, D., 2002. Convective support of long-wavelength topography in the Appennines (Italy), *Terra Nova,* **11,** 228–233.

de Chabalier, J.B., Lyon-Caen, H., Zollo, A., Deschamps, A., Bernard, P. & Hatzfeld, D., 1992. A detailed analysis of microearthquakes in western Crete from digital three-component seismograms, *Geophys. J. Int.,* **110,** 347–360.

Endrun, B., Meier, T., Bischoff, M. & Harjes, H.-P., 2004. Lithospheric structure in the area of Crete constrained by receiver functions and dispersion analysis of Rayleigh phase velocities, *Geophys. J. Int.,* **158,** 592–608.

Engdahl, E.R., R.D.Van der Hilst, & Buland, R.P., 1998. Global teleseismic earthquake relocation with improved travel times and procedures for depth determination, *Bull. seism. Soc. Am.,* **88,** 722–743.

Engdahl, E.R., Jackson, J.A., Myers, S.C., Bergman, E.A. & K. Priestley, 2006. Relocation and assessment of seismicity in the Iran region, *Geophys. J. Int.,* **167,** 761–778.

Fitch, T.J., 1970. Earthquake Mechanisms in the Himalayan, Burmese, and Andaman Regions and Continental Tectonics in Central Asia, *JGR,* **75,** 2699–2709.

Foucher, J.P., N., Chamot-Roocke, Alexandry, S., Augustin, J.M., Monti, S., Pavlakis, P. & Voisset, M., 1993. Multibeam bathymetry and seabed reflectivity maps of the MEDRIFF corridor across the eastern Mediterranean Ridge, *Terra Cognita (Ed.)*, EUG (VII), London, Blackwell Scientific Publication: 278–279.

Frohlich, C., 1989. The nature of deep-focus earthquakes, *Ann. Rev. Earth planet. Sci.,* **17,** 227–254.

Ganas, A. & Parsons, T., 2009. Three-dimensional model of Hellenic Arc deformation and origin of the Cretan uplift, *J. geophys. Res.,* **114,** doi:10.1029/2008JB005599.

Ganas, A. *et al.*, 2009. On the Mw 6.4 SW-Achaia (western Greece) earthquake sequence of 8 June 2008: seismological, field, GPS observations and stress modeling, *J. Earthq. Eng.,* **13,** 1101–1124.

Goldsworthy, M. & Jackson, J., 2000. Active normal fault evolution in Greece revealed by geomorphology and drainage patterns, *J. Geol. Soc.,* **157,** 967–981.

Goldsworthy, M., Jackson, J. & Haines, J., 2002. Continuity of active fault systems in Greece, *Geophys. J. Int.,* **148,** 596–618.

Guidoboni, E. & Comastri, A., 1997. The large earthquake of 8 August 1303 in Crete: seismic scenario and tsunami in the Mediterranean, *J. Seismol.,* **1,** 55–72.

Guidoboni, E. & Comastri, A., 2005. Catalogue of earthquakes and tsunamis in the Mediterranean area from the 11th to the 15th century, *Istituto Nazionale di Geofisica e Vulcanologia*.

Hatzfeld, D., 1994. On the shape of the subducting slab beneath the Peleponnese, Greece, *Geophys. Res. Lett.,* **21,** 173–176.

Hatzfeld, D. & Martin, C., 1992. Intermediate depth seismicity in the Aegean defined by teleseismic data, *Earth planet. Sci. Lett.,* **113,** 267–275.

Hatzfeld, D., Pedotti, G., Hatzidimitriou, P. & Makropoulos, K., 1990. The strain pattern in the western Hellenic arc deduced from a microearthquake survey, *Geophys. J. Int.,* **101,** 181–202.

Hatzfeld, D., Besnard, M., Makropoulosw, K. & Hatzidimitriou, P., 1993. Microearthquake seismicity and fault-plane solutions in the southern Aegean and its geodynamic implications, *Geophys. J. Int.,* **115,** 799–818.

Hollenstein, C., Mller, M., Geiger, A. & Kahle, H.-G., 2008. Crustal motion and deformation in Greece from a decade of GPS measurements, 1993-2003, *Tectonophysics,* **449**(1–4), 17–40.

Huguen, C., Mascle, J., Chaumillon, E., Woodside, J.M., Benkhelil, J., Kopf, A. & Volkonskaia, A., 2001. Deformational styles of the eastern Mediterranean Ridge and surroundings from combined swath mapping and seismic reflection profiling, *Tectonophysics,* **343,** 21–47.

Hyndman, R.D., Yamano, M. & Oleskevich, D.A., 1997. The seismogenic zone of subduction thrust faults, *Island Arcs,* **6,** 244–260.

Isacks, B. & Molnar, P., 1969. Mantle earthquake mechanisms and the sinking of the lithosphere, *Nature,* **223,** 1121–1124.

Jackson, J., 1994. Active tectonics of the Aegean Region, *Annu. Rev. Earth planet. Sci.,* **22,** 239–271.

Jackson, J. & McKenzie, D., 1988. The relationship between plate motions and seismic moment tensors, and rates of active deformation in the Mediterranean and Middle East, *Geophys. J.,* **93,** 45–73.

Kanamori, H., 1977. Seismic and aseismic slip along subduction zones and their tectonic implications, in *Island Arcs, Deep Sea Trenches and Back-Arc Basins, Maurice Ewing Ser. 1*, pp. 163–174, eds Talwani, M. and Pitman, W.C., III, AGU, Washington, DC.

Kastens, K.A., Nancy, A.B. & Cita, M.B., 1992. Progressive deformation of an evaporite-bearing accretionary complex: Sea-MARCI, SeaBeam and piston core observations from the Mediterranean Ridge, *Mar. Geophys. Res.,* **14,** 249–298.

Kelletat, D. & Gassert, D., 1975. Quartarmorphologische Untersuchungen im Kustenraum der Mani Halbinsel, Peleponnes, *Z. Geom. N. F, Suppl.,* **22,** 8–56.

Kenyon, N.H., Belderson, R.H. & Stride, A.H., 1982. Detailed tectonic trends on the central part of the Hellenic outer ridge and in the Hellenic trench system, *Geol. Soc. Lond.,* **10,** 335–343.

Kiratzi, A. & Louvari, E., 2003. Focal mechanisms of shallow earthquakes in the Aegean Sea and the surrounding lands determined by waveform modelling: a new database, *J. Geodyn.,* **36**(1–2), 251–274. Active Faults: Analysis, Processes and Monitoring.

Kiratzi, A. *et al.*, 2008. The April 2007 earthquake swarm near Lake Trichonis and implications for the active tectonics in western Greece, *Tectonophysics,* **452,** 51–65.

Kokinou, E., Papadimitriou, E., Karakostas, V., Kamberis, E. & Vallianatos, F., 2006. The Kefalonia Transform Zone (offshore Western Greece) with special emphasis to its prolongation towards the Ionian Abyssal Plain, *Mar. Geophys. Res.,* **27,** 241–252.

Konstantinou, K., Melis, N., Lee, S.-J., Evangelidis, C. & Boukouras, K., 2009. Rupture process and aftershocks relocation of the 8 june 2008 mw 6.4 earthquake in northwest Peloponnese, western Greece, *Bull. seism. Soc. Am.,* **99,** 3374–3389. doi:10.1785/0120080301.

Kreemer, C. & Chamot-Rooke, N., 2004. Contemporary kinematics of the southern Aegean and the Mediterranean Ridge, *Geophys. J. Int.,* **157,** 1377–1392.

Le Pichon, X., 1982. Landlocked oceanic basins and continental collision: the Eastern Mediterranean as a case example, in *Mountain Building Processes*, pp. 201–211, ed. Hsü, K., Academic Press, London.

Le Pichon, X. & Angelier, J., 1981. The Aegean Sea, *Phil. Trans. Roy. Soc. Lond. Ser. A, Math. Sci.,* **300,** 357–372.

Le Pichon, X. *et al.*, 1979. From subduction to transform motion: a seabeam survey of the Hellenic trench system, *Earth planet. Sci. Lett.,* **44,** 441–450.

Le Pichon, X., Lyberis, N., Angelier, J. & Renard, V., 1982. Strain distribution over the East Mediterranean Ridge: a synthesis incorporating new Sea-Beam data, *Tectonophysics,* **86,** 243–274.

Le Pichon, X., Lallemant, S.J., Chamot-Rooke, N., Lemeur, D. & Pascal, G., 2002. The Mediterranean Ridge backstop and the Hellenic nappes, *Mar. Geol.,* **186,** 111–125.

Li, X. *et al.*, 2003. Receiver function study of the Hellenic subduction zone: imaging crustal thickness variations and the oceanic Moho of the descending African lithosphere, *Geophys. J. Int.,* **155,** 733–748.

Louvari, E., Kiratzi, A.A. & Papazachos, B.C., 1999. The Cephalonia Transform Fault and its extension to western Lefkada Island (Greece), *Tectonophysics,* **308,** 223–236.

Lyon-Caen, H. *et al.*, 1988. The 1986 Kalamata (south Peloponnesus) earthquake: detailed study of a normal fault, evidences for east-west extension in the Hellenic arc, *J. geophys. Res.,* **93,** 14 967–15 000.

Maggi, A., Jackson, J.A., McKenzie, D. & Priestley, K., 2000a. Earthquake focal depths, effective elastic thickness, and the strength of the continental lithosphere, *Geology,* **28,** 495–498.

Maggi, A., Jackson, J.A., Priestley, K. & Baker, C., 2000b. A re-assessment of focal depth distributions in southern Iran, the Tien Shan and northern India: do earthquakes really occur in the continental mantle? *Geophys. J. Int.,* **143,** 629–661.

Mascle, J. & Chaumillon, E., 1998. An overview of Mediterranean Ridge collisional accretionary complex as deduced from multichannel seismic data, *Geo-Mar. Lett.,* **18,** 81–89.

Mattei, M., D'Agostino, N., Zananiri, I., Kondopoulou, D., Pavlides, S. & Spatharas, V., 2004. Tectonic evolution of fault-bounded continental blocks: comparison of Paleomagnetic and GPS data in the Corinth and Megara basins (Greece), *J. geophys. Res.,* **109,** B02106, doi:10.1029/2003JB002506.

McCaffrey, R., 1996. Slip partitioning at convergent plate boundaries of SE Asia, *Geol. Soc., Lond., Special Publications,* **106,** 3–18.

McCaffrey, R. & Abers, G., 1988. SYN3: a program for inversion of teleseismic body waveforms on microcomputers, *Air Force Geophysics Laboratory Technical Report*, AFGL-TR-88-0099: Hanscomb Air Force Base, MA.

McCaffrey, R. & Nabelek, J., 1987. Earthquakes, gravity, and the origin of the Bali Basin: an example of a nascent continental fold-and-thrust belt, *J. geophys. Res.,* **92,** 441–460.

McCaffrey, R., Zwick, P. & Abers, G., 1991. SYN4 Program, *IASPEI Software Library,* **3,** 81–166.

McClusky, S., 2000. Global positioning system constraints on plate kinematics and dynamics in the eastern Mediterranean and Caucasus, *J. geophys. Res.,* **105,** 5695–5719.

McKenzie, D., 1972. Active Tectonics of the Mediterranean Region, *Geophys. J. R. astr. Soc.,* **30,** 109–185.

McKenzie, D., 1978. Active Tectonics of the Alpine-Himalayan belt: the Aegean Sea and surrounding regions, *Geophys. J. Int.,* **55,** 217–254.

McKenzie, D., 2003. Estimating T_e in the presence of internal loads, *J. geophys. Res.,* **108,** 2438.

McKenzie, D. & Jackson, J., 1983. The relationship between strain rates, crustal thickening, palaeomagnetism, finite strain and fault movements within a deforming zone, *Earth planet. Sci. Lett.,* **65,** 182–202.

McQuarrie, N., Stock, J.M., Verdel, C. & Wernicke, B.P., 2003. Cenozoic evolution of Neotethys and implications for the causes of plate motions, *Geophys. Res. Lett.,* **30,** doi:10.1029/2003GL017992.

Meier, T., Rische, M., Endrun, B., Vafidis, A. & Harjes, H.P., 2004. Seismicity of the Hellenic subduction zone in the area of western and central Crete observed by temporary local seismic networks, *Tectonophysics,* **383,** 149–169.

Molnar, P. & Lyon-Caen, H., 1989. Fault plane solutions of earthquakes and active tectonics of the Tibetan Plateau and its margins, *Geophys. J. Int.,* **99,** 123–153.

Nabelek, J.L., 1984. Determination of earthquake source parameters from inversion of body waves, *PhD thesis*, MIT, MA.

Nothard, S., McKenzie, D., Haines, J. & Jackson, J., 1996. Gaussian curvature and the relationship between the shape and the deformation of the Tonga slab, *Geophys. J. Int.,* **127,** 311–327.

Papazachos, B.C., Karakostas, V.G., Papazachos, C.B. & Scordilis, E.M., 2000. The geometry of the Wadati-Benioff zone and lithospheric kinematics in the Hellenic Arc, *Tectonophysics,* **319,** 275–300.

Papazachos, B.S., 1996. Large seismic faults in the Hellenic arc, *Ann. Geophys.,* **39,** 892–903.

Pe-Piper, G. & Piper, D.J.W., 2007. Neogene backarc volcanism of the Aegean: new insights into the relationship between magmatism and tectonics, *Geol. Soc. Am.,* Special Paper **418,** 17–31.

Pirazzoli, P.A., Laborel, J. & Stiros, S.C., 1996. Earthquake clustering in the Eastern Mediterranean during historical times, *J. geophys. Res.,* **101,** 6083–6097.

Reilinger, R. *et al.*, 2006. GPS constraints on continental deformation in the Africa-Arabia-Eurasia continental collisional zone and implications for the dynamics of plate interactions, *J. geophys. Res.,* **111,** B05411, doi:10.1029/2005JB004051.

Reilinger, R., McClusky, S., Paradissis, D., Ergintav, S. & Vernant, P., 2009. Geodetic constraints on the tectonic evolution of the Aegean region and strain accumulation along the Hellenic subduction zone, *Tectonophysics,* doi:10.1016/j.tecto.2009.05.027.

Ruff, L. & Kanamori, H., 1983. Seismic coupling and uncoupling at subduction zones, *Tectonophysics,* **99,** 99–117.

Sandwell, D.T. & Smith, W.H.F., 2009. Global marine gravity from retracked geosat and ers-1 altimetry: Ridge segmentation versus spreading rate, *J. Geophys. Res.,* **114,** B01411. doi:10.1029/2008JB006008.

Scheffers, A., Kelletat, D., Vott, A., May, S.M. & Scheffers, S., 2008. Late Holocene tsunami traces on the western and southern coastlines of the Peloponnesus (Greece), *Earth planet. Sci. Lett.,* **269,** 271–279.

Scholz, C.H., 1998. Earthquakes and friction laws. *Nature,* **391,** 37–42,

Shaw, B. *et al.*, 2008. Eastern Mediterranean tectonics and tsunami hazard inferred from the AD 365 earthquake, *Nat. Geosci.,* **1,** 268–276.

Smith, W.H.F. & Sandwell, D.T., 1997. Global seafloor topography from satellite altimetry and ship depth soundings, *Science,* **277,** 1957–1962.

Spakman, W., Wortel, M.J.R. & Vlaar, N.J., 1998. The Hellenic subduction zone: a tomographic image and its geodynamic implications, *Geophys. Res. Lett.,* **15,** 60–63.

Stern, R.J., 2002. Subduction zones, *Rev. Geophys.,* **40,** 3–1.

Stiros, S. & Drakos, A., 2006. A fault model for the tsunami-associated, magnitude > 8.5 Eastern Mediterranean, AD 365 Earthquake, *Zeitschrift fur Geomorphologie,* **146,** 125–137.

Talebian, T. & Jackson, J., 2004. A reappraisal of earthquake focal mechanisms and active shortening in the zagros mountains of iran, *Geophys. J. Int.,* **156,** 506–526.

Taymaz, T., Jackson, J. & Westaway, R., 1990. Earthquake mechanisms in the Hellenic Trench near Crete, *Geophys. J. Int.,* **102,** 695–731.

Taymaz, T., Jackson, J. & McKenzie, D., 1991. Active tectonics of the north and central Aegean Sea, *Geophys. J. Int.,* **106,** 433–490.

Walker, R., Jackson, J. & Baker, C., 2003. Surface expression of thrust faulting in eastern iran: source parameters and surface deformation of the 1978 tabas and 1968 ferdows earthquake sequences, *Geophys. J. Int.,* **152,** 749–765.

Wortel, R., 1982. Seismicity and rheology of subducted slabs, *Nature,* **296,** 553–556.

Wortel, R., 1986. Deep earthquakes and the thermal assimilation of subducting lithosphere, *Geophys. Res. Lett.,* **13,** 34–37.

Zwick, P., McCaffret, R. & Abers, G., 1994. MT5 program, *IASPEI Software Library 4*.

APPENDIX: EARTHQUAKE DEFICIT CALCULATION

We can calculate the expected seismic moment release rate in the Hellenic subduction zone if it is fully coupled, using the known rate of convergence between Nubia and the Southern Aegean. The total along-strike length of the arc is 600 km, and the convergence rate is 35 mm yr^{-1} (Reilinger *et al.* 2006). Focal mechanisms of earthquakes in Fig. 7 show that the subduction zone interface dips at 15° and that the deepest earthquakes on it occur at a depth of 40 km. The downdip width of the seismogenic interface is therefore 40/sin15°, or 155 km. Since seismic moment, $M_o = \mu As$, where μ is the rigidity modulus (3×10^{10} Pa s), A is the area of the fault plane, and s is slip along the fault plane, we can estimate the moment release rate that we would expect if earthquakes accommodated all of the Nubia-Aegean motion to be 97×10^{18} N m yr^{-1}.

Several authors (Jackson & McKenzie 1988; Ganas & Parsons 2009), have estimated the average rate of moment released in earthquakes, averaged over the last 100 yr or less, to be between 3×10^{18} and 19×10^{18} N m yr^{-1}, which is much less than the above fully-coupled requirement.

We can check, update and refine these estimates of the seismically released moment over the last 100 yr. The catalogue of Jackson & McKenzie (1988) is claimed to be complete above M_w 6.0 between 1908 and 1981, but the locations and depths of the earlier earthquakes in this catalogue are not well determined. They separated earthquakes that occurred near the Hellenic trench into two categories: those with probable shallow focal depths (which might contribute to the convergence), and earthquakes with deeper focal depths that are probably related to deformation within the subducting slab. Even if we consider only the apparently shallow earthquakes, the moment release obtained is likely to be an upper bound on the true moment release, because we now know that some of them accommodate along-strike shortening or extension of the downgoing or overriding material and not convergence in the subduction zone itself. If we extend the catalogue to 2009, and then allow for the additional contribution of earthquakes with $M_w < 6.0$ (Cowie & Scholz 1992), we estimate an observed average seismic moment release rate over the last 100 yr of between 7.4×10^{18} and 15.8×10^{18} N m yr^{-1}, depending on whether we include only the apparently shallow earthquakes, or all of those from the catalogue of Jackson & McKenzie (1988), including those that might be deep. This equates to between 8 per cent and 16 per cent of the Nubia-Aegean motion, confirming the substantial seismic moment deficit inferred by earlier authors.

Thus, over the last 100 yr, earthquakes have been unable to account for at least 85 per cent of the moment required to accommodate the known Nubia-Aegean convergence. If this deficit is to be made up by occasional big earthquakes it would require an earthquake of M_w 7.1 every year, or an earthquake of M_w 8.0 earthquake every 14 yr. Only two events of $M_w \sim 8$ are known in the last 2000 yr, in AD 365 and AD 1303. Even if an AD 365-type event of M_w 8.3–8.5 occurs every 900 yr, which Shaw *et al.* (2008) believe to be possible, the moment release rate from such large events is only 5×10^{18} N m yr^{-1}. These rare very large events may therefore take up another 5–10 per cent of the moment release, but it is inconceivable that the remaining 75 per cent or more could have been released seismically without being noted in the region's rich historical record (Guidoboni & Comastri 2005; Ambraseys 2009).

GPS velocities in the region also confirm that the subduction zone interface must be largely uncoupled: the Cyclades are moving towards Nubia at only 1 mm yr^{-1} faster than Western Crete (Shaw *et al.* 2008). If the subduction zone interface were locked, there would be a much greater difference in velocity, since Crete would be attached to the downgoing plate and there would be contraction of ∼30 mm yr^{-1} between Crete and the Cyclades.

SUPPORTING INFORMATION

Additional Supporting Information may be found in the online version of this article:

Supplement. Tables of focal parameters of earthquakes discussed in this paper.

Please note: Wiley-Blackwell are not responsible for the content or functionality of any supporting materials supplied by the authors. Any queries (other than missing material) should be directed to the corresponding author for the article.